

Flow induced by the rotation of two circular cylinders in a viscous fluid

E. Dormy¹ and H.K. Moffatt²

¹Département de Mathématiques et Applications, UMR-8553, École Normale Supérieure, CNRS, PSL University, 75005 Paris, FRANCE

²Department of Applied Mathematics and Theoretical Physics, Wilberforce Road, Cambridge CB3 0WA, UK

(Received xx; revised xx; accepted xx)

The Stokes flow driven by the rotation of two parallel cylinders of equal unit radius is determined by both numerical and analytical techniques. A numerical (finite-element) solution is obtained by enclosing the system in an outer cylinder of radius $R_0 \gg 1$, on which different boundary conditions can be imposed. With a gap 2ε between the inner cylinders, attention is focused on the small gap situation $\varepsilon \ll 1$ when lubrication theory becomes applicable. Good agreement with the numerical solution is obtained for both counter-rotating and co-rotating cases. In the counter-rotating situation, the total force F (per unit axial length) acting on the cylinders is determined. Numerical evidence is presented for the conclusion (confirmed by a model calculation in Appendix B) that $F \sim (\log R_0)^{-1}$ as $R_0 \rightarrow \infty$. An exact analytic solution is obtained in the contact limit $\varepsilon = 0$, and a ‘contact force’ in F_c is identified, which contributes to the torque that each cylinder experiences about its axis. The far-field torque doublet (‘torquelet’) is also identified. The manner in which the flow topology adapts to the change in topology of the fluid domain when the cylinders are brought into contact is noted. The ‘sliced-cylinder’ situation when $\varepsilon < 0$ is also considered, and in this case a ‘distributed contact force’ is identified, and a similarity solution is found that describes the flow near the corner singularities. In the case of co-rotating cylinders, the theory of Watson (1995, *Mathematika*, **42**, 105–126) (with $R_0 \rightarrow \infty$) is elucidated and shown to agree well with the numerical solution and with lubrication theory when $\varepsilon \lesssim 0.01$. The (dimensionless) torque $\mathcal{T}(\varepsilon)$ generated by the co-rotation of the cylinders is determined, with asymptotic value $\mathcal{T}(\varepsilon) \sim 17.2587$ as $\varepsilon \downarrow 0$. An alternative exact analytic solution in the contact limit $\varepsilon = 0$ is obtained, for which the torque is zero and the far-field flow is one of uniform (rigid-body) rotation; in a rotating frame of reference in which the fluid at infinity is at rest, the relative flow in this case is identified as a ‘radial quadrupole’.

Key words: Stokes flow, finite elements, lubrication, singularity, contact force, torque, torquelet, ciliary propulsion, radial quadrupole

CONTENTS

1. Introduction	2
2. The case of counter-rotating cylinders	5
2.1. Numerical solution	5
2.2. Lubrication theory	6

2.3. Contact force	11
2.4. Analytic solution when $\varepsilon = 0$	12
2.5. Contact force confirmed	14
2.6. Torque on the cylinders	16
2.7. Note on the neglect of inertia	17
3. Sliced cylinders in contact, with counter-rotation ($\varepsilon < 0$)	17
3.1. Distributed contact force	19
3.2. Corner flow for overlapping cylinders	20
4. The case of co-rotating cylinders	22
4.1. Lubrication approach	22
4.2. Analytic solution when $\varepsilon > 0$	22
4.3. Analytic solution for the case of contact $\varepsilon = 0$	26
4.4. Rotating frame solution; radial quadrupole	27
5. The co-rotating ‘conveyor-belt’ situation when $\varepsilon < 0$	28
6. Conclusions	28
Appendix A	29
A.1. Counter-rotating cylinders	29
A.2. Co-rotating cylinders	31
Appendix B	32
Appendix C	34
Appendix D	37

1. Introduction

The problem of determining the two-dimensional steady Stokes flow induced by the rotation of two parallel cylinders of infinite length in a viscous fluid of infinite extent was initiated in the seminal work of Jeffery (1922), who used bipolar coordinates and conformal transformation in his investigation. He concluded that it was impossible to satisfy the condition that the fluid velocity should vanish ‘at infinity’. The situation was in some respects reminiscent of the classical problem of viscous flow past a circular cylinder, for which Stokes had himself established that there is no solution of the linearised equations satisfying the required condition at infinity (see Lamb 1932, Batchelor 1967, and for resolution by matched asymptotic expansion, Proudman & Pearson 1957). For ease of reference, some aspects of Jeffery’s approach are summarised in Appendix A.

The two-cylinder problem was revisited by Watson (1995) who addressed Jeffery’s paradox, recognising that there may be a self-induced force and/or couple per unit axial length on the pair of cylinders resulting from their rotation. For the case of counter-rotating cylinders, a force may well be generated inducing a two-dimensional stokeslet contribution in the far flow field. Watson argued that the resulting flow should be matched asymptotically to an outer solution of the full Navier-Stokes equations, presumably a jet of the type first analysed by Bickley (1937), but he encountered great difficulties in achieving this. We reconsider the counter-rotating problem in §§2 and 3 (and through a model problem in Appendix B), and we shall provide compelling evidence for the conclusion that the force is actually zero, so that Watson’s proposed remedy is in fact inapplicable.

The counter-rotating problem had been discussed earlier by Dorrepaal, O’Neill & Ranger (1984) supplementing their investigation (by image techniques) of the flow due to either a concentrated line vortex or a line stokeslet outside a stationary circular cylinder. For the counter-rotating problem, they showed on the basis of Jeffery’s (1922) solution

that the force on each cylinder is indeed zero provided Jeffery's uniform streaming at infinity is included. The problem was further investigated by Elliott, Ingham & El Bashir (1995a,b) who, using the boundary element method (BEM), determined the flow for several choices of cylinder radii and angular velocities, with the conclusion that in general "the total force and the total torque [on the pair of cylinders] are both zero". This conclusion was at some variance with the conclusions of Watson (1995), published almost simultaneously. Watson (1995) further pointed out that Smith (1991) had introduced a term proportional to $r^2 \log r$ in the far-field streamfunction; since the corresponding pressure is not single-valued, the matching procedure proposed by Smith is rendered invalid.

A further approach to the two-cylinder problem was adopted by Ueda et al. (2003), who supposed that the two cylinders are abruptly set in motion at time $t = 0$ in an initially quiescent fluid. Neglecting non-linear inertia effects (i.e. for vanishingly small Reynolds number) and using again the boundary element method, they studied the approach to a steady state as $t \rightarrow \infty$, and found expressions for the asymptotic force acting on each cylinder. Among other conclusions, they write that "two counter-rotating identical cylinders of opposite angular velocities $\omega_2 = -\omega_1 \dots$ experience the same and very simple 'drag' ". In this situation these drags must indeed be equal (by symmetry), but there is no suggestion in this statement that they are in fact zero. If they are non-zero (as one might infer from figure 4 and figure 6(b) of this paper) so that the total force on the pair of cylinders is non-zero, then there is an apparent conflict with the assertion of Elliott, Ingham & El Bashir (1995b) quoted above. The situation is indeed confusing, and calls for clarification, which we attempt to provide in the present paper.

For the case of co-rotating cylinders, rotating about their axes which are assumed fixed, there seems little doubt that a torque *is* generated. Watson (1995) showed that, when this torque is properly incorporated, the condition of vanishing velocity at infinity *can* be satisfied; the resulting streamfunction had a complicated form involving infinite series, and Watson made no attempt to describe detailed properties of the flow thus determined. We reconsider this co-rotating problem in §§4 and 5, and review some aspects of Watson's solution in Appendix C.

We shall use dimensionless variables such that the two cylinders $\mathcal{C}_{1,2}$ have equal unit radius and are centred at $(\mp(1 + \varepsilon), 0)$; the gap between the cylinders is thus 2ε , and the boundaries are

$$\mathcal{C}_1 : (x + 1 + \varepsilon)^2 + y^2 = 1 \quad \text{and} \quad \mathcal{C}_2 : (x - 1 - \varepsilon)^2 + y^2 = 1. \quad (1.1)$$

We shall be particularly concerned with the 'small-gap situation' $0 < \varepsilon \ll 1$ and the 'contact limit' $\varepsilon = 0$. The seemingly artificial situation of 'overlapping cylinders' ($\varepsilon < 0$) can in principle be realised with the use of conveyor belts (or by ciliary action in the case of micro-organisms); this turns out to be of interest, and will also be considered.

The problem of satisfying the boundary condition at infinity can be circumvented by supposing that the fluid is bounded externally by a cylinder \mathcal{C}_0 of radius $r = R_0 \gg 1$, on which an appropriate boundary condition can be imposed; this is needed for the numerical treatment presented in this paper, and is in any case more realistic in experimental contexts. We note the comprehensive numerical and experimental investigation by Hills (2002) of the 'two-roll mill' flow in a finite domain with a rectangular outer boundary. Hills used finite-difference techniques with focus on the effects of increasing Reynolds number and of change in the ratio of the cylinder angular velocities.

The topology of two-dimensional flows of this kind in a multiply-connected bounded domain \mathcal{D} is of some interest, as discussed in detail by Jana et al. (1994) (see also Boyland, Aref & Stremmer 2000). It is normal to first locate the stagnation points of such flows

which may be either elliptic points (extrema) or saddle points; these are stationary points of the streamfunction ψ of the flow. If n_e is the number of extrema (maxima or minima of ψ) and n_s is the number of saddle points, then $N_E(\mathfrak{D}) \equiv n_e - n_s$ is a topological invariant that depends only on the topology of the domain \mathfrak{D} , with the qualification that if a streamline terminates on the boundary $\partial\mathfrak{D}$, this must be counted as a ‘boundary-saddle point’ (a ‘parabolic point’ in the terminology of Jana et al. 1994) contributing $+\frac{1}{2}$ to n_s ; such boundary-saddle points must occur in pairs. The ‘Euler constant’ $N_E(\mathfrak{D})$ takes the value 1, 0 or -1 according as \mathfrak{D} is simply-, doubly- or triply-connected. For our two-cylinder problem, the triply-connected domain becomes doubly-connected when the cylinders \mathcal{C}_1 and \mathcal{C}_2 are brought into contact, and it is interesting to see just how it is that the streamline topology adapts to the resulting change of $N_E(\mathfrak{D})$.

In the Stokes approximation, valid at small Reynolds number, the pressure field p and velocity field $\mathbf{u} = (u, v) = (\partial\psi/\partial y, -\partial\psi/\partial x)$ satisfy the equations

$$\mu\nabla^2\mathbf{u} = \nabla p, \quad \nabla \cdot \mathbf{u} = 0, \quad (1.2)$$

where μ is the dynamic viscosity; by rescaling pressure p , we may set $\mu = 1$, and we shall use related non-dimensional variables throughout. The vorticity $\boldsymbol{\omega} = \nabla \times \mathbf{u} = -\nabla^2\psi \mathbf{e}_z$ satisfies $\nabla^2\boldsymbol{\omega} = 0$, so that ψ satisfies the biharmonic equation

$$\nabla^4\psi = 0. \quad (1.3)$$

The no-slip condition is to be satisfied on both \mathcal{C}_1 and \mathcal{C}_2 . We suppose that \mathcal{C}_2 rotates with unit clockwise (dimensionless) angular velocity $\omega_2 = -1$. Then for the counter-rotating case \mathcal{C}_1 rotates anti-clockwise with angular velocity $\omega_1 = +1$, and for the co-rotating case clockwise with $\omega_1 = -1$. Since the equations (1.2) are linear, the general case is simply a linear combination of these two; moreover, the reversibility theorem implies that if the boundary velocities are reversed in sign, then the flow simply reverses ($\mathbf{u} \rightarrow -\mathbf{u}$) everywhere. In the limiting situation $\varepsilon = 0$, the cylinders make contact, and a singularity at the point of contact is to be expected.

Concerning the force and torque results in the unbounded-fluid situation, it may be helpful if we here summarise in simple terms the conclusions that will emerge from our detailed analysis that follows. First, as regards the counter-rotating situation $\omega_1 = -\omega_2$, if the cylinders are free of any external force, then they will ultimately move relative to the fluid with uniform dimensionless velocity $V (= \frac{1}{2}(1 + \varepsilon)^{-1})$ in the y -direction (like two parallel line vortices of circulations $\pm\Gamma$ separated by distance $2d$ in an inviscid fluid which propagate with velocity $V = \Gamma/4\pi d$); in a frame of reference moving with the cylinders, there is thus a uniform streaming velocity $(0, -V)$ at infinity. If on the other hand, in fluid at rest at infinity, we start the rotation impulsively at time $t = 0$ while holding the cylinder axes fixed, a force $(0, F(t))$ is required for $t \geq 0$ to maintain this situation; however a streaming flow $(0, -V)$ is then generated (as surmised by Jeffery 1922) which ultimately extends to infinity, with the result that $F(t) \rightarrow 0$ as $t \rightarrow \infty$. The ultimate steady state is therefore essentially the same as in the ‘free’ situation, and is well described by Jeffery’s original solution.

The co-rotating situation $\omega_1 = \omega_2$ is quite different: if the cylinders are free in this situation, they will orbit around each other (like two line vortices in an inviscid fluid of the same circulation Γ which orbit around each other with angular velocity $\Omega = \Gamma/4\pi d^2$); in a frame of reference rotating with the cylinder pair, the fluid at infinity is in uniform (rigid-body) rotation, with angular velocity $-\Omega$ (this is the situation described by Jeffery 1922). If, on the other hand, the cylinder rotations are started abruptly, their axes being fixed, then a torque $\mathcal{T}(t)$ on the cylinder pair relative to the origin is required to maintain this situation. This torque is imparted to the fluid and generates a vortex-like flow $u_\theta \sim \mathcal{T}/4\pi r$

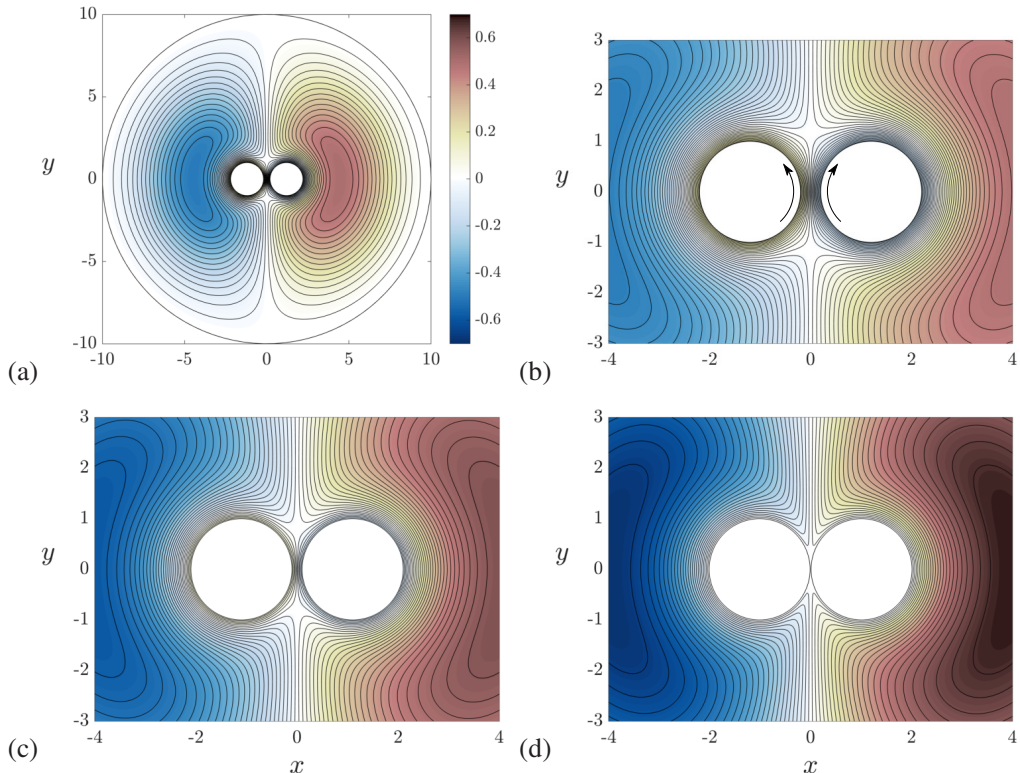


FIGURE 1. Streamlines $\psi = \text{const.}$ from the numerical solution of the Stokes problem for counter-rotating cylinders; the outer boundary condition is no slip on $r = R_0$ (here $R_0 = 10$); the colour code is the same for all four panels. (a) $\varepsilon = 0.2$, full flow domain; (b) $\varepsilon = 0.2$, zoom to neighbourhood of inner cylinders; the sense of rotation is indicated by the arrows; (c) same zoom for $\varepsilon = 0.1$; (d) same zoom for $\varepsilon = 0.01$. Note that the two saddle points on the y -axis approach the origin as ε decreases.

which ultimately extends to infinity, and the torque \mathcal{T} asymptotes to a constant non-zero value (just as would be required for a single cylinder rotating in a fluid at rest at infinity). There is no rigid-body ingredient in this flow, and it is therefore quite distinct from Jeffery’s ‘free’ situation. It is in fact correctly described by Watson’s (1995) theory.

In the following sections, we provide a full justification of these assertions.

2. The case of counter-rotating cylinders

2.1. Numerical solution

Consider first the counter-rotating case with non-dimensionalised boundary conditions

$$\omega_1 = 1 \text{ on } \mathcal{C}_1, \quad \omega_2 = -1 \text{ on } \mathcal{C}_2, \quad \mathbf{u} = 0 \text{ on } \mathcal{C}_0. \quad (2.1)$$

We used a finite-element procedure (details in Appendix D) to provide an accurate numerical solution. Figure 1(a) shows the streamlines $\psi = \text{const.}$ for the flow when $\varepsilon = 0.2$ and $R_0 = 10$. Note the presence of two saddle points near the inner cylinders on the y -axis. There are also two boundary-saddle points where the y -axis meets the boundary \mathcal{C}_0 , each contributing $\frac{1}{2}$ to n_s , so $n_s = 3$ for this configuration. There are two

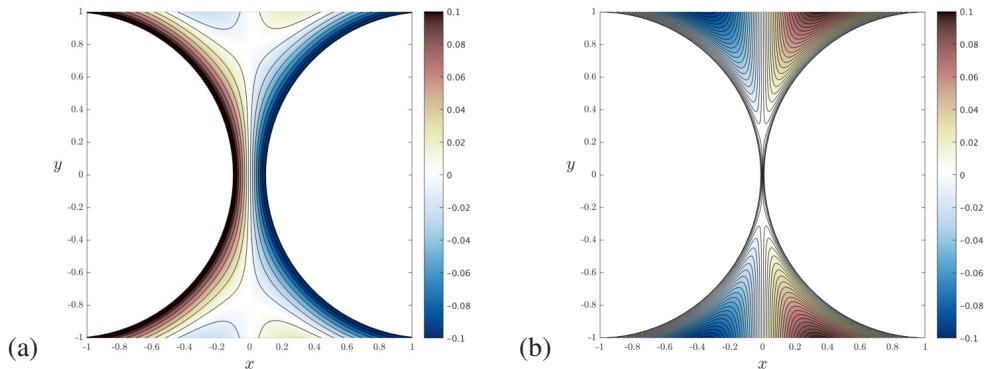


FIGURE 2. As for figure 1(c,d), further zoomed to near the origin; (a) $\varepsilon = 0.1$; (b) $\varepsilon = 0.01$.

elliptic stagnation points on the x -axis, so $n_e = 2$, and $n_e - n_s = N_E(\mathfrak{D}) = -1$, as must be the case for this triply-connected domain of fluid.

The interior saddle points are more evident in the zoom of figure 1(b). There is an upward flux in the gap between the cylinders, and the flow due to the rotation of each cylinder may exert an upward drag force on the other. The cylinders then jointly exert an equal and opposite (downward) force on the fluid; when R_0 is finite, this creates a stokeslet contribution to the flow beyond the cylinders, the possibility recognised by Watson (1995); (we shall however show that this force and the associated stokeslet decrease slowly to zero as $R_0 \rightarrow \infty$). This is coupled with the downward streaming previously found by Jeffery (1922). The downward flow opposes the upward flow through the gap, leading to the presence of the two saddle points.

Figure 1(c) shows the same zoom when ε is reduced to 0.1. Note here how the saddle points have moved closer to the origin, a process that is further marked in figure 1(d) for which $\varepsilon = 0.01$. The zoom of figure 2(a) to the neighbourhood of the origin for the case $\varepsilon = 0.1$ makes this even more evident; figure 2(b) for $\varepsilon = 0.01$ shows that the saddle points are now well within the narrow gap where lubrication theory should be relevant. We shall find in §2.2 below that the saddle points are located at $y = \pm(6\varepsilon)^{1/2}$ as $\varepsilon \rightarrow 0$ (see below equation (2.14)).

In the contact limit $\varepsilon = 0$, the two interior saddle points are replaced by two boundary saddle points at $x = 0, y = \pm 0$. Each contributes $\frac{1}{2}$ to n_s , so that now $n_s = 2$ and $n_e - n_s = 0$, correct for this now doubly-connected fluid domain.

2.2. Lubrication theory

If we assume that $0 < \varepsilon \ll 1$, then lubrication theory should be applicable and reasonably accurate in the gap region. In this region, the surfaces of the two cylinders are at $x = \pm h(y)$, where

$$h(y) = \varepsilon + \frac{1}{2}y^2 + O(y^4), \quad dh/dy = y + O(y^3). \quad (2.2)$$

In the lubrication approximation (Batchelor 1967, §4.8), $p = p(y)$ and (still setting $\mu = 1$)

$$\frac{dp}{dy} = \frac{\partial^2 v}{\partial x^2}, \quad (2.3)$$

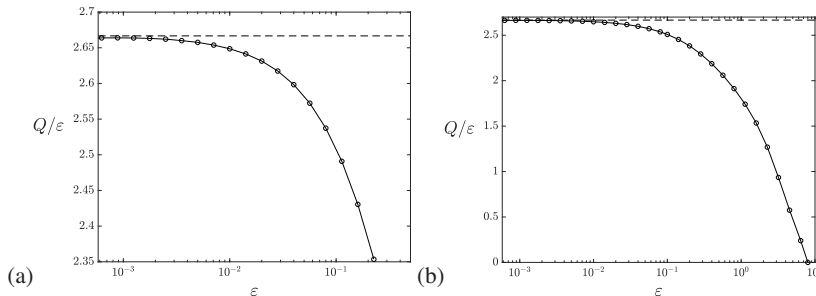


FIGURE 3. (a) Normalised mass flux Q through the small gap between the cylinders as a function of ε ; the dashed asymptote is at $Q/\varepsilon = 8/3 = 2.66\dots$, as determined by lubrication theory (equation (2.9)); (b) showing that, as ε increases to its limiting value (8 for $R_0 = 10$) when $\mathcal{C}_{1,2}$ make contact with \mathcal{C}_0 , the normalised mass flux decreases to zero.

where $\mathbf{u} = (u, v)$ with $|v| \gg |u|$. This integrates with boundary conditions $v = \cos y \approx 1$ on $x = \pm h(y)$ to give

$$v(x, y) = 1 + \frac{1}{2} \frac{dp}{dy} (x^2 - h(y)^2). \quad (2.4)$$

The flux Q between the cylinders is then

$$Q = \int_{-h(y)}^{h(y)} v(x, y) dx = 2h(y) - \frac{2}{3} \frac{dp}{dy} h(y)^3, \quad (2.5)$$

so that

$$\frac{2}{3} \frac{dp}{dy} = \frac{2}{h(y)^2} - \frac{Q}{h(y)^3} = \frac{2}{(\varepsilon + \frac{1}{2}y^2)^2} - \frac{Q}{(\varepsilon + \frac{1}{2}y^2)^3}. \quad (2.6)$$

This integrates to give the deviation of pressure from the pressure p_0 ‘at infinity’ as

$$p(y) = -\frac{3Qy}{2\varepsilon(y^2 + 2\varepsilon)^2} - \frac{3(3Q - 8\varepsilon)}{8\varepsilon^2} \left[\frac{y}{y^2 + 2\varepsilon} + \frac{1}{\sqrt{2\varepsilon}} \tan^{-1} \left[\frac{y}{\sqrt{2\varepsilon}} \right] \right]. \quad (2.7)$$

For large $|y|$, (2.7) gives

$$p(y) \sim \pm \frac{3\pi(3Q - 8\varepsilon)}{16\sqrt{2}\varepsilon^{5/2}} + O(|y|^{-3}), \quad (2.8)$$

and since $p(y) \rightarrow 0$ for large $|y|$, the leading term must vanish, giving

$$Q = 8\varepsilon/3. \quad (2.9)$$

As expected, $Q \rightarrow 0$ as $\varepsilon \rightarrow 0$.

The flux Q as a function of ε , computed from the numerical solution of §2.1, is shown in figure 3(a,b) in which the asymptote at $Q/\varepsilon \sim 8/3 \approx 2.666$ is shown by the dashed line. The behaviour here gives confidence that lubrication theory is indeed reliable when $\varepsilon \ll 1$, and that the flow in the gap is well resolved by the numerical solution for values of ε down to a few 10^{-5} . For smaller values, numerical resolution becomes more challenging, but the lubrication description becomes increasingly accurate.

With $Q = 8\varepsilon/3$, (2.6) and (2.7) give

$$\frac{dp}{dy} = \frac{1}{h(y)^2} \left(3 - \frac{4\varepsilon}{h(y)} \right), \quad (2.10)$$

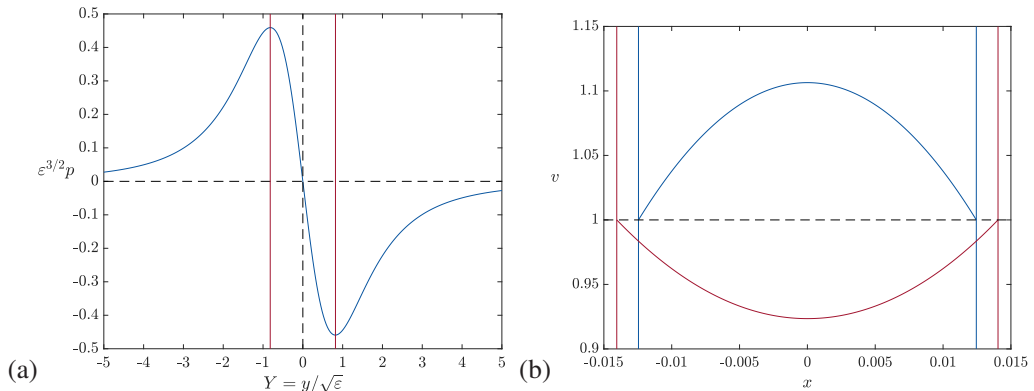


FIGURE 4. (a) Plot of $\varepsilon^{3/2}p(Y)$ vs $Y = y/\sqrt{\varepsilon}$ as given by (2.11); (b) velocity profiles (equation (2.12)) for $\varepsilon = 10^{-2}$ at two sections, $y = 0.7\varepsilon^{1/2}$ (blue) and $y = 0.9\varepsilon^{1/2}$ (red); the boundaries are at $x = \pm h(y)$ in each case, and diverge as y increases; the viscous wall stress is positive for $y < 0.816\varepsilon^{1/2}$, negative for $y > 0.816\varepsilon^{1/2}$.

and, with $Y = y/\sqrt{\varepsilon}$,

$$p(y) = -\frac{4y}{(y^2 + 2\varepsilon)^2}, \quad \text{or equivalently} \quad \varepsilon^{3/2}p(Y) = -\frac{4Y}{(Y^2 + 2)^2}; \quad (2.11)$$

and (2.4) gives

$$v(x, y) = 1 + \frac{1}{2h(y)^2} \left(3 - \frac{4\varepsilon}{h(y)} \right) (x^2 - h(y)^2). \quad (2.12)$$

Using the suffix L to denote the lubrication approximation, the corresponding stream-function $\psi_L(x, y)$, satisfying $\partial\psi_L/\partial x = -v(x, y)$ and $\psi_L(0, y) = 0$, is

$$\psi_L(x, y) = -x - \frac{1}{2h(y)^2} \left(3 - \frac{4\varepsilon}{h(y)} \right) \left(\frac{1}{3}x^3 - h(y)^2x \right). \quad (2.13)$$

The scaled pressure as a function of $Y = y/\sqrt{\varepsilon}$ is shown in figure 4(a). The singular behaviour $p(y) \sim -4y^{-3}$ when $\varepsilon = 0$ is unphysical, and indicates that in practice some deformation of the cylinders must occur if they are brought into contact while rotating, a phenomenon first recognised by Hertz (1882). The singularity in pressure could presumably be resolved by taking such deformation into account. This resolution problem lies outside the scope of the present treatment, and will be ignored in what follows.

The pressure gradient (2.10) is negative for $h(y) < 4\varepsilon/3$, i.e. for $|y| < (2\varepsilon/3)^{1/2} \approx 0.816\varepsilon^{1/2}$. It follows from (2.3) that the curvature of the velocity profile across the gap changes sign at $|y| \approx 0.816\varepsilon^{1/2}$. Figure 4(b) shows two velocity profiles across the gap, the blue one at $y = 0.7\varepsilon^{1/2}$, just below the critical level at which the curvature changes sign, the red one at $y = 0.9\varepsilon^{1/2}$ just above. The wall stress below the critical level $y = 0.816\varepsilon^{1/2}$ evidently provides a positive contribution to the force on the cylinders, while above this critical level, it provides a negative contribution.

The velocity on the axis $x = 0$ is

$$v(0, y) = 1 + \frac{1}{2} \left(\frac{4\varepsilon}{h(y)} - 3 \right) = \frac{2\varepsilon}{h(y)} - \frac{1}{2} = \frac{4}{2 + Y^2} - \frac{1}{2}. \quad (2.14)$$

This vanishes where $h(y) = 4\varepsilon$, i.e. at $|Y| = \sqrt{6}$, or $|y| = (6\varepsilon)^{1/2} \approx 2.45\varepsilon^{1/2}$; this therefore, as previously stated, gives the location of the two saddle points on the y -axis.

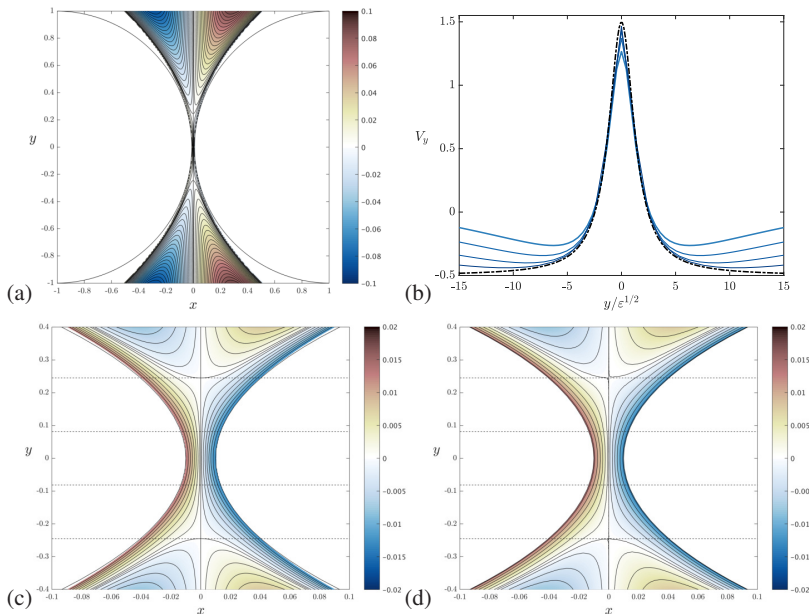


FIGURE 5. (a) Streamlines $\psi_L(x, y) = \text{const.}$ as given by (2.13) for the case $\varepsilon = 0.01$ (compare with figure 2b); (b) vertical velocity on the mid-plane $v(0, Y)$, where $Y = y/\sqrt{\varepsilon}$, for $\varepsilon = 0.2, 0.1, 0.05, 0.025$, with correspondingly decreasing line thickness; the solution determined by lubrication theory (equation (2.14)) is shown in black, dash-dotted; (c) same as (a), but closer to the origin and with x -coordinate stretched by a factor 4; (d) the same from the full numerical solution, with the same colour code; the difference is almost imperceptible. The critical levels $y = \pm 0.816 \varepsilon^{1/2}$ and $y = \pm 2.45 \varepsilon^{1/2}$ are shown by the dashed lines.

Figure 5(a) shows the streamlines $\psi_L = \text{const.}$ given by (2.13) for $\varepsilon = 0.01$, which admits comparison with the numerical solution shown in figure 2(b). Figure 5(c) shows the same nearer the origin with the x -coordinate stretched by a factor 4, and figure 5(d) shows the same streamlines as determined by the full numerical solution; the difference here is almost imperceptible, again giving confidence in the accuracy of both the numerics and the lubrication theory at least at this value of $\varepsilon = 0.01$. In both panels, the critical levels $y = \pm 0.816 \varepsilon^{1/2}$ (at which the viscous wall stress changes sign) and $y = \pm 2.45 \varepsilon^{1/2}$ (at which the saddle points occur) are shown by the dashed lines.

Figure 5(b) shows the vertical velocity on the mid-plane $v(0, Y)$, where $Y = y/\sqrt{\varepsilon}$, for $\varepsilon = 0.2, 0.1, 0.05, 0.025$, with correspondingly decreasing line thickness, and the limiting curve (dash-dotted) as given by lubrication theory (equation (2.14)). The curves shadow the limiting curve ever more faithfully as ε decreases, giving further confidence in the relevance of the limiting lubrication-theory treatment.

Figure 6(a) shows the streamlines in the gap as given by (2.13) for the even smaller value $\varepsilon = 0.001$, and figure 6(b) shows the same zoomed near the origin and stretched in the x -direction, again revealing the saddle-point structure.

2.2.1. Force on the cylinders, as determined by lubrication theory

The vertical force F_y on each cylinder consists of two parts: (i) the shear stress (viscous) force F_{yv} and (ii) the pressure force F_{yp} ; for $\varepsilon > 0$, these are given by

$$F_{yv} = - \int_{-\infty}^{\infty} \left. \frac{\partial v}{\partial x} \right|_{x=h(y)} dy = \int_{-\infty}^{\infty} \frac{4\varepsilon - 6y^2}{(y^2 + 2\varepsilon)^2} dy = -\pi(2/\varepsilon)^{1/2}, \quad (2.15)$$

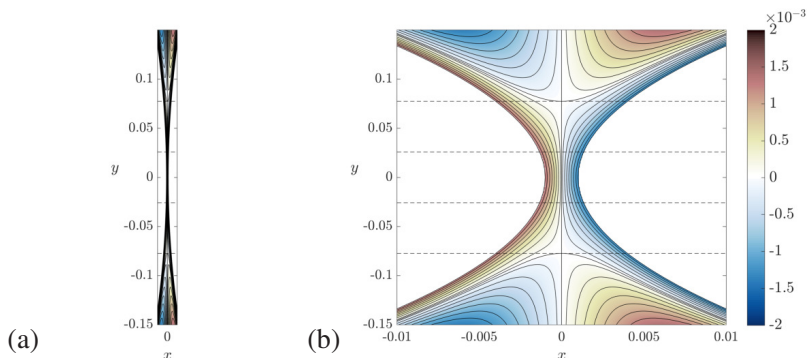


FIGURE 6. Streamlines $\psi_L(x, y) = \text{const.}$ as given by (2.13), for the case $\varepsilon = 0.001$; (a) correct aspect ratio for this value of ε ; (b) zoomed near the origin and stretched in the x -direction, to show more details of the structure; the critical levels $y = \pm 0.816 \varepsilon^{1/2}$ and $y = \pm 2.45 \varepsilon^{1/2}$ are again shown by the dashed lines.

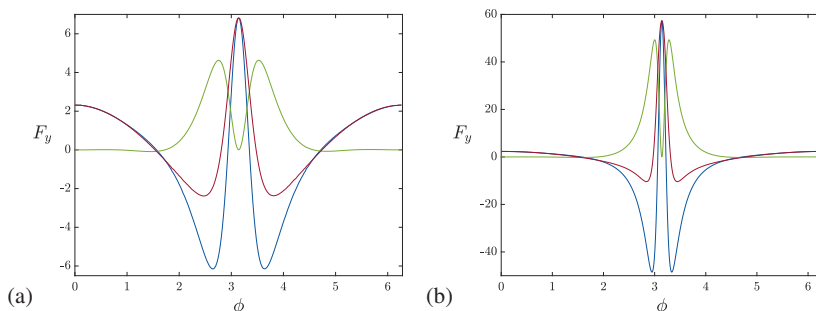


FIGURE 7. Distribution of the vertical forces on \mathcal{C}_2 as functions of the angle ϕ ; the narrowest point of the gap is at $\phi = \pi$; $R_0 = 10$; viscous term (blue), pressure term (green), total force (red); (a) $\varepsilon = 10^{-1}$; (b) $\varepsilon = 10^{-2}$.

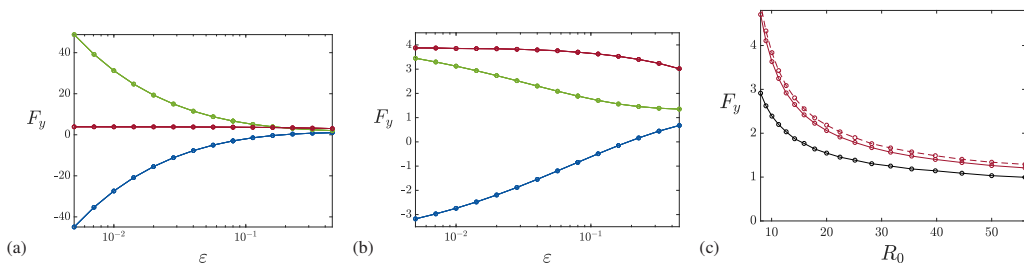


FIGURE 8. (a) Integrated contributions to the vertical force on \mathcal{C}_2 , viscous (blue), pressure (green) and the total (red), as functions of ε ; (b) the same, but with the viscous and pressure contributions rescaled by $\sqrt{\varepsilon}$; (c) dependence of total force on R_0 , $\varepsilon = 0.01$ (solid); no-slip condition on \mathcal{C}_0 (red), stress-free condition on \mathcal{C}_0 (black).

and

$$F_{yp} = \int_{-\infty}^{\infty} p \left(-\frac{dh}{dy} \right) dy = \int_{-\infty}^{\infty} \frac{4y^2}{(y^2 + 2\varepsilon)^2} dy = \pi(2/\varepsilon)^{1/2}, \quad (2.16)$$

so that

$$F_{yv} + F_{yp} = \int_{-\infty}^{\infty} \frac{4\varepsilon - 2y^2}{(y^2 + 2\varepsilon)^2} dy = 0. \quad (2.17)$$

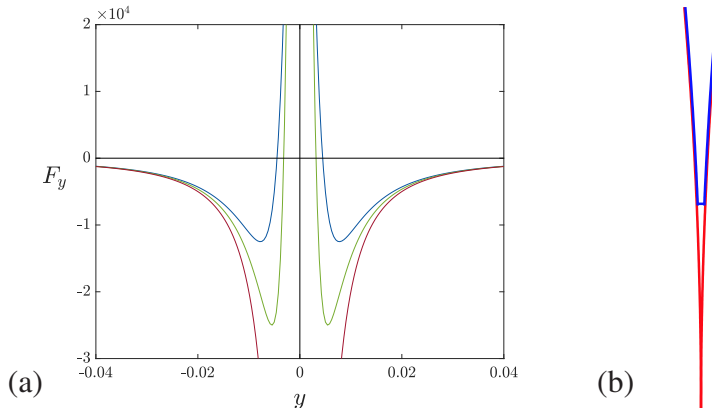


FIGURE 9. (a) Plot of the function $(4\varepsilon - 2y^2)/(y^2 + 2\varepsilon)^2$, for $\varepsilon = 10^{-5}$ (blue), 5×10^{-6} (green) and $\varepsilon = 0$ (red). As $\varepsilon \downarrow 0$, the spike at $y = 0$ becomes longer and narrower, and ultimately disappears in the limit $\varepsilon = 0$; (b) contour (shown in blue) used for calculation of the contact force when $\varepsilon = 0$; the short segment is at the level $y = y_1$, and the limit $y_1 \downarrow 0$ is considered.

Thus, somewhat surprisingly, the total force on each cylinder vanishes at $O(\varepsilon^{-1/2})$. This conclusion is however supported by the numerical solution: figure 7 shows the distribution of the two contributions to the vertical force as functions of the angle ϕ round \mathcal{C}_2 , confirming that the forces are indeed increasingly concentrated near the minimum gap position $\phi = \pi$ as ε decreases; and figure 8 shows that when $R_0 = 10$ the integrated pressure and viscous contributions do indeed nearly cancel at $O(\varepsilon^{-1/2})$, but that there is an $O(1)$ residual contribution $F_{yv} + F_{yp} \approx 3.9$ for $0 < \varepsilon \ll 1$, a result that lies outside the scope of the lubrication approximation. We might expect that this residual force should decrease to zero as R_0 increases without limit, in conformity with Jeffery's (1922) conclusion; figure 8(c) shows that the force does decrease at least in the range $8 < R_0 < 55$. For reasons given in Appendix B, it is almost certain that the force does indeed tend to zero like $(\log R_0)^{-1}$ as $R_0 \rightarrow \infty$, i.e. extremely slowly. Watson's (1995) invocation of a nonzero force in this limit is therefore at the least questionable.

But what if $\varepsilon = 0$? In this situation, when the cylinders make contact, the integrand in (2.17) is $-2/y^2$, and the integral diverges. The force $F_{yv} + F_{yp}$ is then apparently infinite! The situation can be understood with reference to figure 9, which shows a plot of the integrand in (2.17) for $\varepsilon = 10^{-5}$ (blue), 5×10^{-6} (green) and $\varepsilon = 0$ (red). As ε decreases the curves approach the limit curve more and more closely. The spike in the region $|y| < (2\varepsilon)^{1/2}$ contributes the positive value to the integral that exactly compensates the negative value from the region $|y| > (2\varepsilon)^{1/2}$. When $\varepsilon = 0$, the spike disappears, and only the negative contribution survives.

However, in this limit situation when the cylinders make contact, there is a pressure discontinuity across the point of contact, and this can contribute a 'contact force' F_c to the resultant total force on the two cylinders. This contact force can be obtained as follows.

2.3. Contact force

We need simply consider the restricted domain of fluid inside the blue contour shown in figure 9(b) for the contact situation $\varepsilon = 0$ with $h(y) = \frac{1}{2}y^2$. The short segment in this

figure is at the level $y = y_1$. The total force on the curved parts of the blue contour is

$$2 \int_{y_1}^{\infty} \frac{(-2y^2)}{y^4} dy = -\frac{4}{y_1}. \quad (2.18)$$

From (2.11), when $\varepsilon = 0$, the pressure is given by $p = -4/y^3$, so the pressure force on the small horizontal segment (an upwards suction) is

$$\int_{-h(y_1)}^{h(y_1)} -p dx = (4/y_1^3)y_1^2 = +4/y_1. \quad (2.19)$$

This exactly balances the force (2.18) from the curved parts of the contour. (These forces are $\pm 8/y_1$ when contributions from the region $y < 0$ are also taken into account.) This force balance persists in the limit $y_1 \downarrow 0$, and we may conclude that what was the upward contribution to $F_{yv} + F_{yp}$ when $\varepsilon > 0$ is replaced when $\varepsilon = 0$ by the upward contact force resulting from the (infinite) jump in pressure across the point of contact.

The analytic treatment of this limit that now follows provides an alternative derivation of the contact force that does not rely on the lubrication approximation.

2.4. Analytic solution when $\varepsilon = 0$

When $\varepsilon = 0$, the Stokes problem may be solved exactly; this is the limit version of Jeffery (1922) (see Appendix A). Following Schubert (1967), we use the conformal mapping $\zeta \equiv \xi + i\eta = 1/z$, where $z \equiv x + iy$, giving

$$\xi = \frac{x}{x^2 + y^2}, \quad \eta = \frac{-y}{x^2 + y^2}. \quad (2.20)$$

The scale factor for this mapping is

$$h(\xi, \eta) = |d\zeta/dz| = (x^2 + y^2)^{-1} = \xi^2 + \eta^2. \quad (2.21)$$

The contours $\xi = \text{const.}$, $\eta = \text{const.}$ are the circles shown in figure 10(a). The essential property of this mapping is that $\psi(x, y)$ satisfies the biharmonic equation $\nabla^4 \psi = 0$ if and only if $\Psi(\xi, \eta) = h(\xi, \eta)\psi[x(\xi, \eta), y(\xi, \eta)]$ satisfies $\nabla_{\xi, \eta}^4 \Psi = 0$.

For our problem, we want a solution of $\nabla^4 \psi = 0$ that is antisymmetric about $x = 0$, or equivalently a solution of $\nabla_{\xi, \eta}^4 \Psi = 0$ antisymmetric about $\xi = 0$. We also need to impose angular velocities ± 1 on the circles $\xi = \mp 1/2$. The boundary conditions are then

$$\Psi = \Psi_{\xi\xi} = 0 \quad \text{on} \quad \xi = 0, \quad \text{and} \quad \Psi = 0, \quad \Psi_{\xi} = -1 \quad \text{on} \quad \xi = \pm 1/2. \quad (2.22)$$

The required solution evidently does not depend on η ; it is given by

$$\Psi(\xi, \eta) = \xi/2 - 2\xi^3, \quad (2.23)$$

and correspondingly

$$\psi(x, y) = (x^2 + y^2)\Psi(\xi, \eta) = \frac{x}{2} - \frac{2x^3}{(x^2 + y^2)^2}. \quad (2.24)$$

In plane polar coordinates $\{r, \theta\}$, this is equivalently

$$\psi(r, \theta) = \frac{1}{2}r \cos \theta - \frac{3}{2}r^{-1} \cos \theta - \frac{1}{2}r^{-1} \cos 3\theta. \quad (2.25)$$

It may be verified directly that this does indeed satisfy $\nabla^4 \psi = 0$. The leading term $\frac{1}{2}r \cos \theta$ represents a uniform stream $(0, -\frac{1}{2})$, while the term $-\frac{3}{2}r^{-1} \cos \theta$ admits interpretation as the flow due to a vortex dipole (or ‘torque doublet’, or, to coin a suitable word comparable to stokeslet, a ‘torquelet’) $-(\mu/2\pi)\partial \log r/\partial x$, where here $\mu = 3\pi$. The

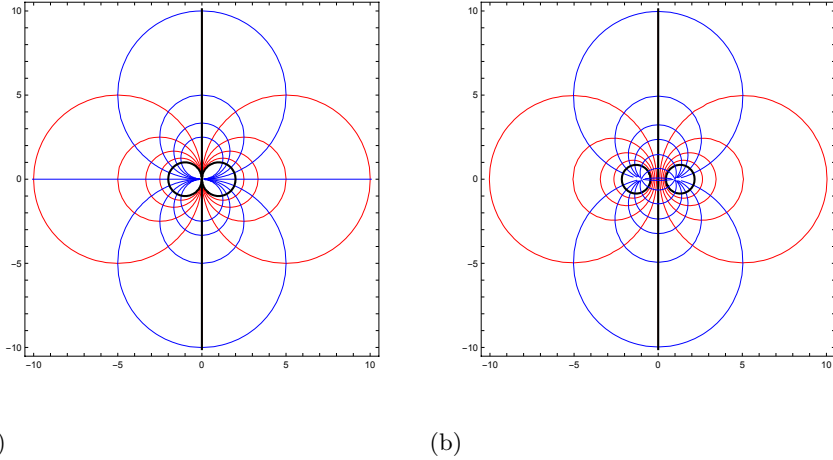


FIGURE 10. (a) Contours $\xi = \text{const.}$ (red) and $\eta = \text{const.}$ (blue), given by (2.20); the contours $\xi = 0, \pm 1/2$ are shown in black; (b) corresponding contours given by the conformal mapping $\zeta = \log[(z + c)/(z - c)]$, as used by Jeffery (1922); here $c = 1$ and the cylinders of unit radius are shown by the contours $\xi = \pm \sinh^{-1} c \approx \pm 0.881$.

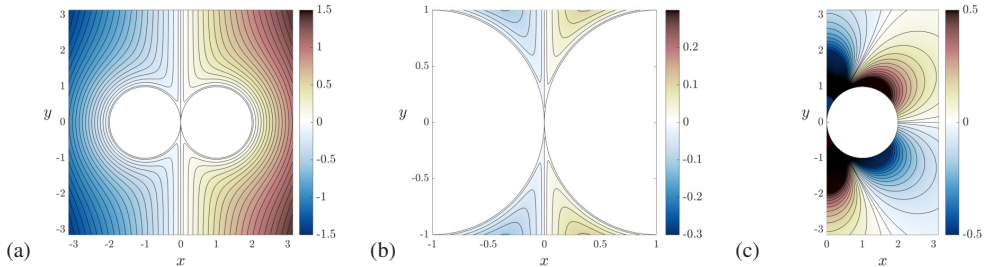


FIGURE 11. (a) Streamlines $\psi = \text{const.}$, as given by (2.24); (b) zoom near the point of contact; (c) contours $p = \text{const.}$ in the half-plane $x > 0$ as given by (2.28).

streamlines $\psi = \text{const.}$ are shown in figure 11(a), and a zoom near the point of contact in figure 11(b).

2.4.1. Pressure field

The velocity components are

$$u(x, y) = \frac{\partial \psi}{\partial y} = \frac{8x^3 y}{(x^2 + y^2)^3}, \quad v(x, y) = -\frac{\partial \psi}{\partial x} = -\frac{1}{2} - \frac{2(x^4 - 3x^2 y^2)}{(x^2 + y^2)^3}. \quad (2.26)$$

The pressure field satisfies the equations

$$\frac{\partial p}{\partial x} = \nabla^2 u = -\frac{48xy(x^2 - y^2)}{(x^2 + y^2)^4}, \quad \frac{\partial p}{\partial y} = \nabla^2 v = \frac{12(x^4 - 6x^2 y^2 + y^4)}{(x^2 + y^2)^4}. \quad (2.27)$$

Either of these equations may be integrated, giving

$$p(x, y) = \frac{4y(3x^2 - y^2)}{(x^2 + y^2)^3}. \quad (2.28)$$

The contours $p(x, y) = \text{const.}$ in the half-plane $x \geq 0$ are shown in figure 11(c).

On the right-hand cylinder \mathcal{C}_2 , let

$$x = 1 + \cos \phi, \quad y = \sin \phi, \quad (-\pi \leq \phi \leq \pi), \quad \text{so } r^2 \equiv x^2 + y^2 = 2(1 + \cos \phi). \quad (2.29)$$

The normal and tangent vectors on \mathcal{C}_2 have cartesian components

$$\mathbf{n} = (\cos \phi, \sin \phi), \quad \mathbf{t} = (-\sin \phi, \cos \phi). \quad (2.30)$$

From (2.28), the pressure on \mathcal{C}_2 is then

$$p(\phi) = \frac{\sin \phi [3(1 + \cos \phi)^2 - \sin^2 \phi]}{2(1 + \cos \phi)^3}. \quad (2.31)$$

The vertical component of the pressure force $-p\mathbf{n}$ on \mathcal{C}_{12} is $-p(\phi)\sin\phi$, which has the asymptotic behaviour

$$-p(\phi)\sin\phi \sim \frac{4}{(\phi - \pi)^2} \quad \text{near } \phi = \pi; \quad (2.32)$$

this is obviously non-integrable at the point of contact $\phi = \pi$.

2.4.2. Viscous stress on cylinder

The rate-of-strain components are

$$e_{11} = \partial u / \partial x, \quad e_{12} = e_{21} = \frac{1}{2}(\partial u / \partial y + \partial v / \partial x), \quad e_{22} = \partial v / \partial y. \quad (2.33)$$

Substituting (2.26), and simplifying leads to the results

$$e_{11}(x, y) = -e_{22}(x, y) = \frac{24y(x^2y^2 - x^4)}{(x^2 + y^2)^4}, \quad e_{12}(x, y) = \frac{6x(x^4 - 6x^2y^2 + y^4)}{(x^2 + y^2)^4}. \quad (2.34)$$

On the cylinder \mathcal{C}_2 with parametric equations (2.29), these reduce to

$$e_{11}(\phi) = -e_{22}(\phi) = \frac{-3\sin 2\phi}{2(1 + \cos \phi)}, \quad e_{12}(\phi) = \frac{3\cos 2\phi}{2(1 + \cos \phi)}. \quad (2.35)$$

The viscous stress components on \mathcal{C}_2 are given by

$$\tau_1(\phi) = 2(e_{11}(\phi)\cos\phi + e_{12}(\phi)\sin\phi), \quad \tau_2(\phi) = 2(e_{21}(\phi)\cos\phi + e_{22}(\phi)\sin\phi), \quad (2.36)$$

and these reduce to

$$\tau_1(\phi) = \frac{-3\sin\phi}{1 + \cos\phi}, \quad \tau_2(\phi) = \frac{3\cos\phi}{1 + \cos\phi}, \quad (2.37)$$

with the asymptotic behaviour near $\phi = \pi$

$$\tau_1(\phi) \sim \frac{6}{\pi - \phi}, \quad \tau_2(\phi) \sim -\frac{6}{(\pi - \phi)^2}. \quad (2.38)$$

Note that the total vertical component of stress on \mathcal{C}_2 , $-p(\phi)\sin\phi + \tau_2(\phi)$, therefore behaves like $-2(\pi - \phi)^{-2}$ near $\phi = \pi$, and is therefore non-integrable, indicating an infinite integrated downward contribution to the vertical force.

2.5. Contact force confirmed

In order to resolve this singularity, we consider the vertical force now integrated round the closed contour shown in red in figure 12, as described in the figure caption. The integral of the vertical force component round \mathcal{C}_2 from $\phi = -\phi_1$ to $\phi = \phi_1$ is, with some

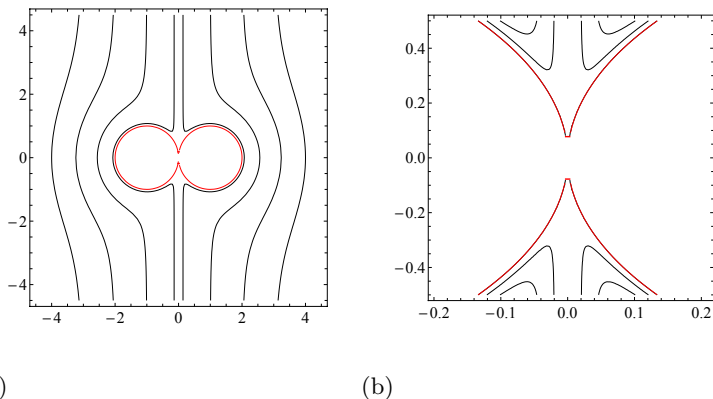


FIGURE 12. (a) Contour of integration (shown in red) for calculating the total resultant vertical force on both cylinders when they make contact ($\varepsilon = 0$); the integral round the right-hand cylinder \mathcal{C}_2 runs from $\phi = -\phi_1$ to $\phi = \phi_1$, where $0 < \pi - \phi_1 \ll 1$ (and this is equal, by symmetry, to the contribution from \mathcal{C}_1); and the integral on the small horizontal segments at $y = \pm y_1$ run from $x = -y_1^2/2$ to $y_1^2/2$, where $y_1 = \sin \phi_1 = \sin(\pi - \phi_1) \sim \pi - \phi_1$; we then take the limit $\phi_1 \rightarrow \pi$ (i.e. $y_1 \rightarrow 0$); (b) zoom near the origin, and expanded by a factor of 4 to make the short sections at $y = \pm y_1$ more clearly visible.

simplification,

$$\int_{-\phi_1}^{\phi_1} (-p(\phi) \sin \phi + \tau_2(\phi)) d\phi = \int_{-\phi_1}^{\phi_1} \frac{2 \cos \phi + \cos 2\phi}{1 + \cos \phi} d\phi = 2 \sin(3\phi_1/2) \sec(\phi_1/2). \quad (2.39)$$

The contribution to $F_{yp} + F_{yv}$ from both \mathcal{C}_1 and \mathcal{C}_2 is therefore

$$4 \sin(3\phi_1/2) \sec(\phi_1/2) \sim -\frac{8}{\pi - \phi_1} + \frac{26(\pi - \phi_1)}{3} + \mathcal{O}(\pi - \phi_1)^3, \quad (2.40)$$

which is indeed singular as $\phi_1 \rightarrow \pi$. However, as in §2.3, there is also a contribution to the total vertical force from the small segments at $y = \pm y_1$; this is

$$F_c = \int_{-h(y_1)}^{h(y_1)} [p(x, -y_1) - p(x, y_1)] dx = \frac{128}{y_1(4 + y_1)^2} \sim \frac{8}{y_1} - 4y_1 + \mathcal{O}(y_1^3), \quad (2.41)$$

and, since $y_1 \sim \pi - \phi_1$, the singularity here exactly cancels the singularity in (2.40) as $y_1 \rightarrow 0$. Moreover since this leaves terms of order y_1 which vanish in the limit, it follows that, in the limit, the total net force on the composite body is zero:

$$F_y = \lim_{y_1 \rightarrow 0} (F_{yp} + F_{yv} + F_c) = 0. \quad (2.42)$$

This is consistent with the result (2.17), implying that the conclusion that the force is zero is in fact valid for all $\varepsilon \geq 0$. This also confirms the validity of the simpler derivation of the same force balance under the lubrication approximation, as presented in §2.3.

We shall see in §2.6.2 below how $\frac{1}{2}F_c$ exerts part of the torque that each cylinder experiences about its axis.

2.5.1. Motion of cylinders relative to the fluid at infinity

Note that in a frame of reference fixed in the fluid at infinity, the two cylinders move with velocity $\mathbf{V} = (0, \frac{1}{2})$. The force generated by their rotation is then equal and opposite

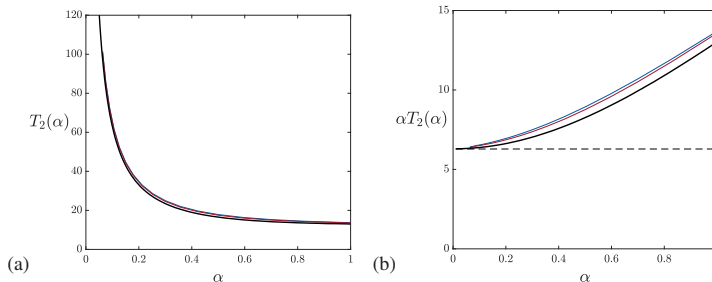


FIGURE 13. (a) The torque $\mathcal{T}_2(\alpha)$ where $\alpha = \cosh^{-1}(1 + \varepsilon) \sim (2\varepsilon)^{1/2}$, computed from the solution of Jeffery (1922) (see Appendix A, in black), and from the full numerics with $R_0 = 10$ (in blue), and $R_0 = 15$ (in red); (b) The function $\alpha\mathcal{T}_2(\alpha)$ with the same color code; the level 2π is shown by the dashed line, showing that $\mathcal{T}_2(\alpha) \sim 2\pi/\alpha = \pi(2/\varepsilon)^{1/2}$ as $\alpha \rightarrow 0$.

to the drag force that they jointly experience as they move through the fluid; in effect the velocity \mathbf{V} is just such that this force balance is exactly satisfied.

2.6. Torque on the cylinders

2.6.1. Torque when $\varepsilon > 0$

Since the total force on each cylinder, including the contact force, is zero (when $R_0 \rightarrow \infty$), the torques $\mathcal{T}_1 \mathbf{e}_z$ and $\mathcal{T}_2 \mathbf{e}_z = -\mathcal{T}_1 \mathbf{e}_z$ acting on $\mathcal{C}_{1,2}$ are independent of the point relative to which the torque is calculated, e.g. \mathcal{T}_2 is the same whether calculated relative to the centre of \mathcal{C}_2 or relative to the origin O . When $0 < \varepsilon \ll 1$, the viscous drag on \mathcal{C}_2 is concentrated near the gap point $(\varepsilon, 0)$ and the pressure on \mathcal{C}_2 makes no contribution to the torque about its axis at $(1 + \varepsilon, 0)$; hence, using (2.15), this torque is given by

$$\mathcal{T}_2 \sim -F_{yv} \sim \pi(2/\varepsilon)^{1/2}. \quad (2.43)$$

Figure 13(a) shows the torque $\mathcal{T}_2(\alpha)$ (where $\alpha \sim (2\varepsilon)^{1/2}$) computed both from our numerical solution for $R_0 = 10$ (blue) and 15 (red), and from the solution of Jeffery (1922) as described in Appendix A (black), and figure 13(b) shows the corresponding compensated functions $\alpha\mathcal{T}_2(\alpha)$. The convergence as R_0 increases is evident, and it is clear that, in the limit $R_0 \rightarrow \infty$, $\mathcal{T}_2(\alpha) \sim 2\pi/\alpha$ as $\alpha \rightarrow 0$, in perfect agreement with the asymptotic result (2.43).

The pair of torques $\pm\mathcal{T}_2(\alpha)$ do indeed constitute a torquelet associated with the term $-\frac{3}{2}r^{-1} \cos \theta$ in (2.25). We shall confirm in Appendix A that (2.25) is the limit as $\varepsilon \rightarrow 0$ of the solution found by Jeffery (1922), and that the torquelet ingredient of this flow, $-\frac{3}{2}r^{-1} \cos \theta$, is associated in the limit $\alpha \sim (2\varepsilon)^{1/2} \rightarrow 0$ with torque singularities $\pm\mathcal{T}_2(\alpha) \sim \pm 2\pi/\alpha$ separated by the vanishing distance $d(\alpha) \sim 3\alpha$ (equation (A 5)).

2.6.2. Torque when $\varepsilon = 0$

When $\varepsilon = 0$, it is instructive also to calculate the asymptotic behaviour of this torque as a function of the cut-off level y_1 defined in figure 12. From the cartesian stress components (2.37), the tangential stress on \mathcal{C}_2 is

$$\tau(\phi) = \tau_2(\phi) \cos \phi - \tau_1(\phi) \sin \phi = 3(1 + \cos \phi)^{-1}. \quad (2.44)$$

Integrating this from $-\phi_1$ to $+\phi_1$ where $\pi - \phi_1 \sim y_1 \ll 1$ gives the moment of this tangential stress as

$$M_v = \int_{-\phi_1}^{\phi_1} \frac{3}{1 + \cos \phi} d\phi = 6 \tan(\phi_1/2) \sim \frac{12}{\pi - \phi_1} \quad \text{as } \phi_1 \rightarrow \pi. \quad (2.45)$$

There is also a contribution from the moment of the half of the contact force F_c that can be deemed to act on \mathcal{C}_2 , viz, $M_c = -\frac{1}{2}F_c \sim -4/y_1$ from (2.41). Combining these moments gives the torque

$$\mathcal{T}_2(y_1) = M_v + M_c \sim 8/y_1 \quad \text{as } y_1 \rightarrow 0, \quad (2.46)$$

and we note again that, by symmetry, $\mathcal{T}_1(y_1) = -\mathcal{T}_2(y_1)$.

Alternatively, we may calculate this same torque relative to the origin O. The tangential stress $\tau(\phi)$ exerts a moment $(\mathbf{x} \times \mathbf{t})\tau(\phi)$ about the contact point O(0, 0); here,

$$\mathbf{x} = (1 + \cos \phi, \sin \phi) \quad \text{and} \quad \mathbf{t} = (-\sin \phi, \cos \phi), \quad \text{so} \quad \mathbf{x} \times \mathbf{t} = (1 + \cos \phi)\mathbf{e}_z, \quad (2.47)$$

and it follows remarkably that this moment takes the value 3, uniform on \mathcal{C}_2 , so that the total moment of the tangential stress about O takes the finite value $M_{Ov} = 3(2\pi) = 6\pi$. However, noting that

$$\mathbf{x} \times \mathbf{n} = (1 + \cos \phi, \sin \phi) \times (\cos \phi, \sin \phi) = \sin \phi \mathbf{e}_z \quad \text{on } \mathcal{C}_2, \quad (2.48)$$

it is actually the pressure $-p(\phi)\mathbf{n}$ on \mathcal{C}_2 that exerts the dominant moment about O; using (2.31) and (2.48), this is

$$M_{Op} = \int_{-\phi_1}^{\phi_1} -p(\phi) \sin \phi \, d\phi = -6\phi + 4 \sin \phi + 4 \tan(\phi/2) \sim \frac{8}{\pi - \phi_1} - 6\pi, \quad (2.49)$$

and so the torque relative to O is

$$\mathcal{T}_2(y_1) = M_{Ov} + M_{Op} \sim 8/y_1 \quad \text{as } y_1 \sim \pi - \phi_1 \rightarrow 0, \quad (2.50)$$

in precise agreement with (2.46). We should note here that the contact force has zero moment about O in the limit $y_1 \rightarrow 0$.

2.7. Note on the neglect of inertia

If we resume dimensional variables with a the radius of the cylinders and $U = |\omega_1|a$ the speed on the rotating cylinder surfaces, the Reynolds number of the flow is $\text{Re} = Ua/\nu$, where ν is the kinematic viscosity of the fluid, and it is assumed that $\text{Re} \ll 1$. The velocity \mathbf{u} given by (2.26) has the form $\mathbf{u} = U(0, -\frac{1}{2}) + O(Ua/r)$ for $r \gg a$. The neglected inertia term $\mathbf{u} \cdot \nabla \mathbf{u}$ in the Navier-Stokes equation is therefore of order $U^2 a/r^2$, whereas the retained term $\nu \nabla^2 \mathbf{u}$ is of order $\nu a U/r^3$. The ratio of the inertia term to the viscous term is therefore of order $\text{Re} r/a$. This is just as for low-Reynolds-number flow past a *sphere*, although in that case the r^{-1} term is associated with a three-dimensional stokeslet. As in that case, an Oseen-type correction to the flow can be obtained in the region $r/a \gtrsim \text{Re}^{-1}$, but we shall not here pursue this refinement, which has no effect on the flow field in the inner region $r/a = O(1)$.

When the flow is confined to the cylinder $r < R_0$, as in figure 1, it is evident that inertia is negligible throughout the fluid domain \mathfrak{D} provided the double inequality $\text{Re} \ll a/R_0 \ll 1$ is satisfied.

3. Sliced cylinders in contact, with counter-rotation ($\varepsilon < 0$)

It is of some interest to consider also the limit as ε approaches zero from below. The situation $\varepsilon < 0$ corresponds to overlapping cylinders. With $\varepsilon_1 = -\varepsilon > 0$, the cylinders intersect at $x = 0$, $y = \pm(2\varepsilon_1)^{1/2}$, and at a finite angle $2\alpha \sim 2(2\varepsilon_1)^{1/2}$. When $\varepsilon_1 \ll 1$, and $y^2 > 2\varepsilon_1$, the fluid boundary in the lubrication region is at $x = \pm h(y)$ where now $h(y) = \frac{1}{2}y^2 - \varepsilon_1$. The situation could be approximated experimentally by using conveyor

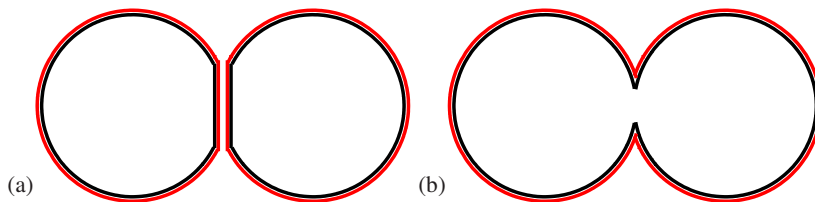


FIGURE 14. ‘Sliced cylinders’ (black) with conveyor belts (red): (a) counter-rotating cylinders simulated with two conveyor belts; if the gap is reduced to zero, then the situation of ‘overlapping cylinders’ with $\varepsilon < 0$ is approximately realised; (b) co-rotating cylinders simulated with a single conveyor belt.

belts around two ‘sliced cylinders’ and bringing the two flat faces together, as illustrated in figure 14(a). In biomechanics, it is a situation that could in principle be realised by ciliary propulsion of a micro-organism (Lighthill 1952; Lauga & Powers 2009). Equally, it is the situation first recognised by Hertz (1882), when two solid elastic bodies are in contact, one rolling on the other.

For $0 < \varepsilon_1 \ll 1$, the velocity profile for $(2\varepsilon_1)^{1/2} < |y| \ll 1$ is still given by equation (2.4), but the flux Q given by (2.9) is now zero so that

$$\frac{dp}{dy} = \frac{3}{h(y)^2} = \frac{12}{(y^2 - 2\varepsilon_1)^2}. \quad (3.1)$$

The pressure $p(y)$ is now therefore given by

$$p(y) = 12 \int \frac{dy}{(y^2 - 2\varepsilon_1)^2}, \quad (3.2)$$

and the y -component of velocity is

$$v(x, y) = \frac{3x^2}{2h(y)^2} - \frac{1}{2}, \quad (3.3)$$

with corresponding streamfunction

$$\psi_L(x, y) = \frac{x}{2} - \frac{x^3}{2h(y)^2}; \quad (3.4)$$

the streamlines $\psi_L = \text{const.}$ are shown in figure 15 for $\varepsilon_1 = 10^{-1}, 10^{-2}$ and 10^{-3} . Obviously the description becomes more accurate as $\varepsilon_1 \downarrow 0$ (i.e. $\varepsilon \uparrow 0$).

With $Y_1 = y/(2\varepsilon_1)^{1/2} > 1$, the integral (3.2) now gives

$$\frac{(2\varepsilon_1)^{3/2}p(y)}{3} = 4 \int \frac{dY_1}{(Y_1^2 - 1)^2} = \frac{-2Y_1}{Y_1^2 - 1} + \log \frac{Y_1 + 1}{Y_1 - 1}. \quad (3.5)$$

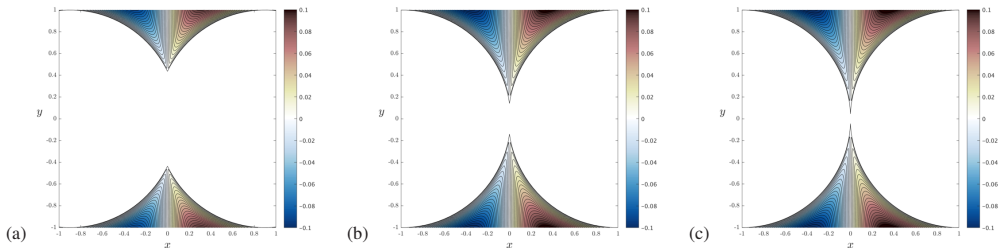
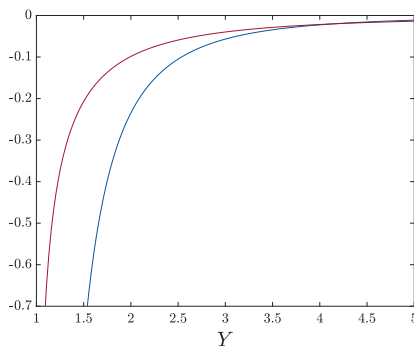
This pressure function is shown by the blue curve in figure 16. The vertical component of the pressure force on the boundary $x = h(y)$ for $y > (2\varepsilon_1)^{1/2}$, i.e. $Y_1 > 1$, is then given by

$$-yp(y) = \frac{3}{\varepsilon_1} \left(\frac{Y_1^2}{Y_1^2 - 1} - \frac{Y_1}{2} \log \frac{Y_1 + 1}{Y_1 - 1} \right). \quad (3.6)$$

The viscous stress on the boundary $x = h(y)$ for $y > (2\varepsilon_1)^{1/2}$ is given by

$$\tau(y) = -\frac{\partial v}{\partial x} = -\frac{6}{y^2 - 2\varepsilon_1} = -\frac{3}{\varepsilon_1(Y_1^2 - 1)}. \quad (3.7)$$

It then follows from (3.6) and (3.7) that the vertical component of total stress on the


 FIGURE 15. Streamlines for the flow (3.4) for $\varepsilon_1 \equiv -\varepsilon = 10^{-1}$, 10^{-2} and 10^{-3} .

 FIGURE 16. The pressure function $-2Y(Y^2 - 1)^{-1} + \log[(Y + 1)/(Y - 1)]$ (blue, equation (3.5)) and the total vertical stress function $1 - \frac{1}{2}Y \log[(Y + 1)/(Y - 1)]$ (red, equation (3.8)).

boundary is

$$\sigma(y) \equiv \tau(y) - yp(y) = 3\varepsilon_1^{-1} \left(1 - \frac{Y_1}{2} \log \frac{Y_1 + 1}{Y_1 - 1} \right). \quad (3.8)$$

Note that the dominant terms of order $(Y_1 - 1)^{-1}$ in (3.6) and (3.7) cancel, leaving the weaker logarithmic singularity at $Y_1 = 1$ in (3.8). (We shall see later (equation (3.22) below) that this singularity must result from the curvature of \mathcal{C}_1 and \mathcal{C}_2 away from the point of intersection $Y_1 = 1$).

The total force from the curved parts of the composite body is now

$$F_{yv} + F_{yp} = 4 \int_{(2\varepsilon_1)^{1/2}}^{\infty} (\tau(y) - yp(y)) dy = 12\sqrt{2} \varepsilon_1^{-1/2} \int_1^{\infty} \left(1 - \frac{Y_1}{2} \log \frac{Y_1 + 1}{Y_1 - 1} \right) dY_1. \quad (3.9)$$

The integrand is shown by the orange curve in figure 16; the singularity at $Y_1 = 1$ is integrable, and as $Y_1 \rightarrow \infty$,

$$1 - \frac{Y_1}{2} \log \frac{Y_1 + 1}{Y_1 - 1} \sim -\frac{1}{3}Y_1^{-2}. \quad (3.10)$$

The integral therefore converges; it actually evaluates to $-\frac{1}{2}$, giving

$$F_{yv} + F_{yp} = -6\sqrt{2} \varepsilon_1^{-1/2}. \quad (3.11)$$

3.1. Distributed contact force

Again however, we have to consider whether the infinite difference in pressure between $y = -(2\varepsilon_1)^{1/2}$ and $y = +(2\varepsilon_1)^{1/2}$ may contribute to the total vertical force on the composite body. To calculate this, consider the pressure $p(y_1)$ at a small distance above $y = (2\varepsilon_1)^{1/2}$ (i.e. above $Y_1 = 1$). This is given by (3.5), and so (allowing also for the

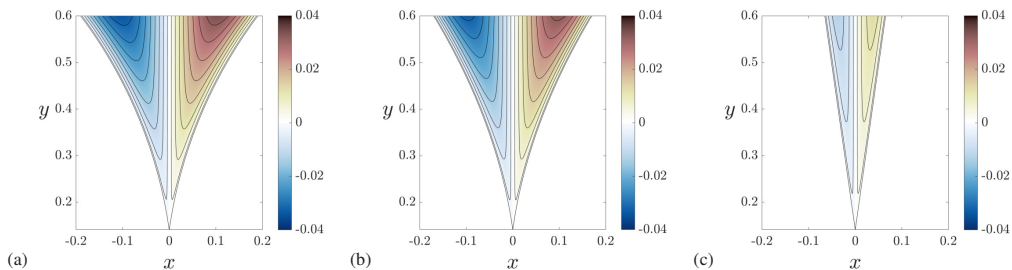


FIGURE 17. (a) Streamlines near the corner for $\varepsilon_1 = 10^{-2}$ ($\alpha = (2\varepsilon_1)^{1/2} = 0.1414$): (a) from the full numerics; (b) from lubrication theory (equation 3.4), and (c) from the local similarity solution (3.14) and (3.18) (with boundaries at $\theta = \pm\alpha$ and the y -axis coinciding with $\theta = 0$). The angle at the singular point $(0, \alpha)$ is 2α , the same in each case.

similar singularity at $Y_1 = -1$)

$$\begin{aligned} F_c &= \lim_{Y_1 \rightarrow 1} \int_{-h(y_1)}^{h(y_1)} [p(-y_1) - p(y_1)] dx \\ &= \frac{6}{(2\varepsilon_1)^{1/2}} \lim_{Y_1 \rightarrow 1} \left\{ 2Y_1 - (Y_1^2 - 1) \log \left[\frac{Y_1 + 1}{Y_1 - 1} \right] \right\} = +6\sqrt{2} \varepsilon_1^{-1/2}, \end{aligned} \quad (3.12)$$

a value that again exactly compensates the contribution (3.11); so again

$$F_{yv} + F_{yp} + F_c = 0. \quad (3.13)$$

Here, the force F_c is due to the finite area of contact of the two sliced cylinders, and may therefore be appropriately described as a ‘distributed contact force’.

3.2. Corner flow for overlapping cylinders

Since, when $\varepsilon < 0$, the cylinders intersect at a finite angle, we can alternatively consider the local similarity solution that exists very near the line of intersection, where the two boundaries can be treated as approximately plane. Using polar coordinates (r, θ) such that the boundaries are (locally) at $\theta = \pm\alpha$, and with radial velocity $V = 1$ on each boundary, we may seek a similarity solution for the corner streamfunction $\psi_C(r, \theta)$ of the form

$$\psi_C(r, \theta) = rVf(\theta), \quad (3.14)$$

with velocity components

$$u_r = r^{-1} \partial \psi_C / \partial \theta = Vf'(\theta), \quad u_\theta = -\partial \psi_C / \partial r = -Vf(\theta). \quad (3.15)$$

Since u_r is evidently an even function of θ , $f(\theta)$ must be odd; the boundary conditions are then satisfied if

$$f(-\theta) = -f(\theta), \quad f(\alpha) = 0, \quad f'(\alpha) = -1. \quad (3.16)$$

The biharmonic equation $\nabla^4 \psi = 0$ has a solution of the form (3.14) provided

$$f(\theta) = A \sin \theta + B \cos \theta + C \theta \sin \theta + D \theta \cos \theta, \quad (3.17)$$

and the conditions (3.16) determine the constants A, B, C, D , giving

$$f(\theta) = \frac{\alpha \cos \alpha \sin \theta - \theta \cos \theta \sin \alpha}{\alpha - \sin \alpha \cos \alpha}. \quad (3.18)$$

A solution of similar form was first found for the ‘paint-scraper’ problem (Taylor 1962).

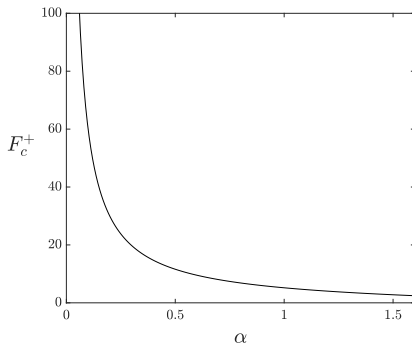


FIGURE 18. Contact force function $F_c^+(\alpha) = 4 \sin^2 \alpha (\alpha - \sin \alpha \cos \alpha)^{-1}$ for corner flow.

Figure 17 shows three panels, (a) showing the local streamline pattern from the full numerical solution for $\varepsilon_1 = 10^{-2}$, (b) showing the corresponding lubrication-theory solution (3.4), and (c) showing the corresponding local similarity solution (3.14) and (3.18) for $\alpha = (2\varepsilon_1)^{1/2} = 0.1414$ (so that the angle at the singular point $(0, \alpha)$ is 2α , the same in each case).

The pressure field $p(r, \theta)$ is given by

$$\frac{\partial p}{\partial r} = \left(\nabla^2 - \frac{1}{r^2} \right) u_r - \frac{2}{r^2} \frac{\partial u_\theta}{\partial \theta}, \quad \frac{1}{r} \frac{\partial p}{\partial \theta} = \left(\nabla^2 - \frac{1}{r^2} \right) u_\theta + \frac{2}{r^2} \frac{\partial u_r}{\partial \theta}. \quad (3.19)$$

Either of these equations leads to the result

$$p(r, \theta) = -\frac{2 \cos \theta \sin \alpha}{r(\alpha - \cos \alpha \sin \alpha)}. \quad (3.20)$$

The tangential (radial) viscous stress on the boundary $\theta = \alpha$ is

$$\tau(r, \alpha) = -\frac{1}{r} \frac{\partial u_r}{\partial \theta} \Big|_{\theta=\alpha} = -\frac{2 \sin^2 \alpha}{r(\alpha - \sin \alpha \cos \alpha)}. \quad (3.21)$$

The total stress on this boundary in the direction $\theta = 0$ is now

$$\sigma(r, \alpha) \equiv \tau(r, \alpha) \cos \alpha - p(r, \alpha) \sin \alpha \equiv 0. \quad (3.22)$$

Thus the pressure force in the direction $\theta = 0$ is exactly balanced by the viscous stress contribution (see the comment in parenthesis following equation (3.8)).

3.2.1. Corner contact force

But consider now, as before, the contact force F_c^+ concentrated at the corner. This is obtained as

$$F_c^+ = \lim_{r \rightarrow 0} \int_{-\alpha}^{\alpha} -p(r, \theta) r \, d\theta = \frac{4 \sin^2 \alpha}{\alpha - \sin \alpha \cos \alpha}. \quad (3.23)$$

The function $F_c^+(\alpha)$ is shown in figure 18. For small α , this suction force has the asymptotic form $F_c^+ \sim 6/\alpha - 4\alpha/5 + O(\alpha^3)$, or, setting $\alpha = (2\varepsilon_1)^{1/2}$,

$$F_c^+ \sim 3\sqrt{2} \varepsilon_1^{-1/2}, \quad (3.24)$$

consistent with the result (3.12) (given that here only the upper singularity is considered; an equal contribution comes from the lower singularity).

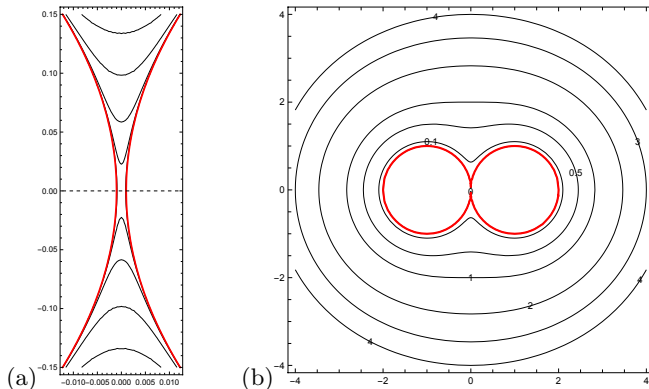


FIGURE 19. (a) Contours $\psi_L(x, y) = \text{const.}$ as given by (4.2), for the case $\varepsilon = 0.001$; (b) contours for the analytic solution (4.12), when the cylinders make contact; here the flow asymptotes to rigid-body rotation with angular velocity $\Omega = -\frac{1}{2}$ as $r \rightarrow \infty$.

4. The case of co-rotating cylinders

4.1. Lubrication approach

If the cylinders are co-rotating, both in the clockwise sense ($\omega_1 = \omega_2 = -1$), the pressure in the gap is uniform, and the lubrication solution for the vertical velocity is very simple: with velocity now ± 1 on the cylinder boundaries $x = \pm h(y) = \pm(\varepsilon + \frac{1}{2}y^2)$, this solution is

$$v(x, y) = \frac{x}{h(y)} = \frac{2x}{2\varepsilon + y^2}, \quad (4.1)$$

and the corresponding streamfunction satisfying $v(x, y) = -\partial\psi_L/\partial x$ is

$$\psi_L(x, y) = \frac{h(y)^2 - x^2}{2h(y)}, \quad (4.2)$$

for which the streamlines $\psi_L = \text{const.}$ are shown in figure 19. The x -component of velocity is

$$u(x, y) = \frac{\partial\psi_L}{\partial y} = y \left[\frac{1}{2} + \frac{2x^2}{(y^2 + 2\varepsilon)^2} \right]. \quad (4.3)$$

Thus, on the y -axis, $u(0, y) = \frac{1}{2}y$; it will turn out that this does correctly represent the flow in the lubrication region $y = O(\varepsilon^{1/2})$ — see figure 21(a) below.

The vertical forces on \mathcal{C}_1 and \mathcal{C}_2 , now due only to the viscous stress on the boundary, are respectively

$$F_y = \mp \int_{-\infty}^{\infty} \frac{dy}{h(y)} = \mp \pi(2/\varepsilon)^{1/2}, \quad (4.4)$$

singular in the limit $\varepsilon \rightarrow 0$. In this limit these forces are located very near the points $(\mp\varepsilon, 0)$, so the torque on each cylinder about its axis is $\mathcal{T} \sim \pi(2/\varepsilon)^{1/2}$. However, the torque relative to the origin $(0, 0)$ acting on the pair of cylinders is $G(\varepsilon) \sim 2\pi(2\varepsilon)^{1/2}$, vanishing in the limit $\varepsilon \rightarrow 0$.

4.2. Analytic solution when $\varepsilon > 0$

Jeffery's (1922) solution for the case of co-rotating cylinders, which also gave zero torque on the cylinder pair, failed to satisfy the desired condition of vanishing velocity at infinity. This 'Jeffery paradox' was addressed by Watson (1995), who compared the situation to the case of a single cylinder rotating in an unbounded fluid, for which the

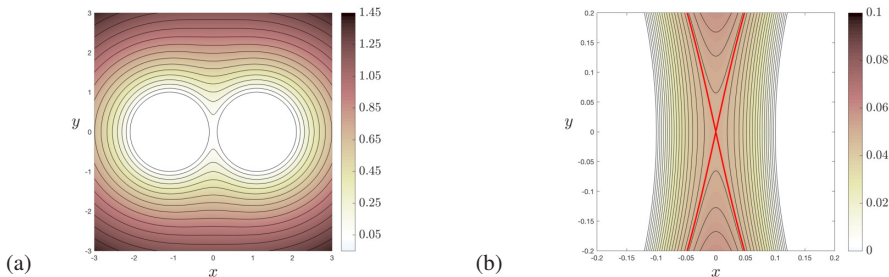


FIGURE 20. (a) Contours $\psi_W(x, y) = \text{const.}$ as given by (C 5) in Appendix C, for the situation when $r_1 = 1$, $\varepsilon = 0.1$ (so $\alpha = 0.4436$, $c = 0.4583$); (b) zoom of the same near the origin, showing in red the expected saddle point where $\psi_W(0, 0) = 0.0491475$.

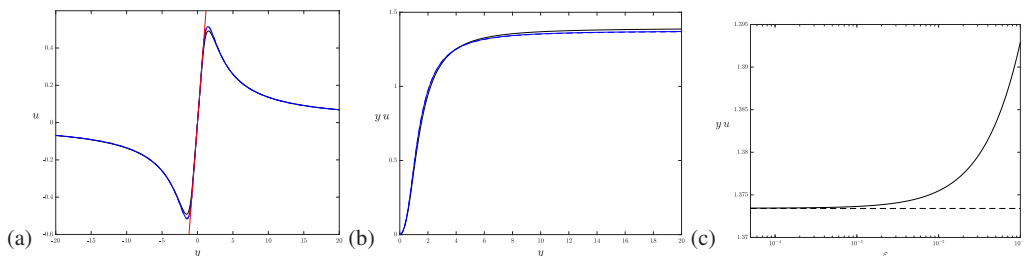


FIGURE 21. (a) Plots of $u_W(0, y)$ for $r_1 = 1$, and $\varepsilon = 0.1$ (solid black), $\varepsilon = 0.01$ (solid blue), $\varepsilon = 0.001$ (dashed blue); the last two curves are indistinguishable on the scale shown. These graphs show the expected behaviour $u_W(0, |y|) \sim |y|^{-1}$ for large $|y|$. The red line has slope $1/2$, and correctly represents the flow in the lubrication region $y = O(\varepsilon^{1/2})$; (b) Corresponding plots of $y u_W(0, y)$ for positive y , showing that in fact $y u_W(0, y) \rightarrow k(\varepsilon)$ as $y \rightarrow \infty$. (c) The function $k(\varepsilon) = \lim_{|y| \rightarrow \infty} |y u_W(0, y)|$, which asymptotes to 1.3734 as $\varepsilon \downarrow 0$; this asymptote is shown by the dashed line, which coincides with the level of $\mathcal{T}(0)/4\pi$ as determined by (4.11).

steady flow is that due to a virtual line vortex at the axis of the cylinder. As Watson said “it seems implausible that the introduction of a second [co-rotating] cylinder would change the character of the motion so drastically [as to replace this asymptotic vortex flow by a rigid body rotation]”.

In resolving this paradox, following Jeffery (1922), Watson used bipolar coordinates defined by a conformal mapping, which we here adopt in the form

$$\zeta \equiv \xi + i\eta = \log \frac{z + c}{z - c} \quad \text{with } z \equiv x + iy, \quad (4.5)$$

so that

$$\xi(x, y) = \frac{1}{2} \log \frac{(x + c)^2 + y^2}{(x - c)^2 + y^2}, \quad \eta(x, y) = \tan^{-1} \left[\frac{x + c}{y} \right] - \tan^{-1} \left[\frac{x - c}{y} \right]. \quad (4.6)$$

The scale factor for this mapping is

$$h(\xi, \eta) = \left| \frac{d\zeta}{dz} \right| = \frac{\cosh \xi - \cos \eta}{c}. \quad (4.7)$$

The contours $\xi(x, y) = \text{const.}$, $\eta(x, y) = \text{const.}$ are shown in figure 10(b). The contour $\xi = \alpha$ is a circle with centre at $(c_1, 0)$ where $c_1 = c \coth \alpha$, and radius $r_1 = c \operatorname{cosech} |\alpha|$. If we fix $r_1 = 1$, then $c = \sinh |\alpha|$, and the separation of the two cylinders is (as before)

2ε , where now $\varepsilon = \cosh \alpha - 1$, i.e.

$$\alpha = \cosh^{-1}(1 + \varepsilon). \quad (4.8)$$

The boundaries $\mathcal{C}_{1,2}$ are taken to be $\xi = \mp\alpha$ with $\alpha > 0$, and the fluid domain is $\mathfrak{D} : \{0 \leq |\xi| < \alpha, -\pi < \eta < \pi\}$.

The essential step in Watson's treatment was to introduce a term proportional to $\log\{(x-c)^2 + y^2\}\{(x+c)^2 + y^2\}$ in the solution, thereby contributing a vortex ingredient $u_\theta = k/r$ to the velocity at infinity and an associated torque acting on the cylinder pair. It was then necessary to satisfy the no-slip conditions on the two cylinders, and to ensure that the rigid-body term is expunged from the solution. The rather complex details are summarised in Appendix C. We provide some diagrams here that help in the interpretation of Watson's results. Denoting his streamfunction by $\psi_W(x, y)$, the contours $\psi_W(x, y) = \text{const.}$ are shown in figure 20(a) for the case $r_1 = 1$, $\varepsilon = 0.1$ (so $\alpha = 0.4436$, $c = 0.4583$); the zoom near the origin in figure 20(b) shows the expected saddle point at the origin.

Figure 21(a) shows the corresponding velocity $u_W(y) = \partial\psi_W/\partial y$ on the axis $x = 0$ for $\varepsilon = 0.1$ ($\alpha = 0.4436$, solid black), $\varepsilon = 0.01$ ($\alpha = 0.1413$, solid blue) and $\varepsilon = 0.001$ ($\alpha = 0.04472$, dashed blue); the last two are indistinguishable on the scale shown; the red line, with slope $1/2$, is as given by the lubrication solution (4.3). Figure 21(b) shows that $|u_W(y)| \sim k|y|^{-1}$ for large $|y|$, as for a point vortex; there is no rigid-body ingredient in this solution. The constant k depends on ε , and may be evaluated numerically as $\lim_{|y| \rightarrow \infty} |y u_W(y)|$; the function $k(\varepsilon)$ is shown in figure 21(c), with the limiting behaviour $k(\varepsilon) \sim 1.3734$ as $\varepsilon \downarrow 0$.

Figure 22 shows numerical solutions of the co-rotating problem with $\varepsilon = 0.01$ for three different conditions on the outer boundary $r = R_0 (= 10)$: (a,d) no-slip; (b,e) stress-free; and (c,f) with the boundary condition $v_\theta = -k(\varepsilon)/R_0$ (with $k(0.01)$ derived from the Watson (1995) solution – see figure 21(c)). Figure 23 shows corresponding plots of the axial velocity distributions $v(x, 0)$ ($2 < x < 10$) and $u(0, y)$ ($-10 < y < 10$). The Watson solution shows the expected r^{-1} behaviour in both plots, and the no-slip solution comes quite close to this.

The stress-free solution is very different; it shows behaviour close to rigid-body rotation, as in the solution originally found by Jeffery (1922). Here we may compare the situation with steady circular Couette flow between coaxial rotating cylinders with no slip on the inner cylinder $r = a$ and with the stress-free condition $d[v_\theta(r)/r]/dr = 0$ on the outer cylinder $r = b$; the solution is rigid body rotation no matter how large b/a may be!

Note that in all three cases shown in figure 22, there is one saddle point at the origin, and no elliptic points: $n_e = 0$, $n_s = 1$, so that trivially $n_e - n_s = N_E(\mathfrak{D}) = -1$.

Torque on cylinder pair

Having expunged the rigid-body term in the general solution, the asymptotic form of $\psi_W(x, y)$ for $r = (x^2 + y^2)^{1/2} \rightarrow \infty$ is indeed found to be that of a line vortex

$$\psi_W(x, y) \sim -2K(\alpha) \sinh^2 \alpha \log(1/r), \quad (4.9)$$

where $K(\alpha)$ is the function defined in Appendix C by (C 1) and (C 3); this corresponds to a torque

$$\mathcal{T}(\alpha) = 8\pi K(\alpha) \sinh^2 \alpha \quad (4.10)$$

exerted by the cylinder pair on the fluid. For small $\varepsilon \sim \frac{1}{2}\alpha^2$, using the asymptotic form (C 4), this implies that

$$\mathcal{T}(\alpha) \sim 8\pi\alpha^2(0.6867\alpha^{-2}) = 17.2587, \quad \text{as } \alpha \rightarrow 0; \quad \text{so } \mathcal{T}(0)/4\pi = 1.3734, \quad (4.11)$$

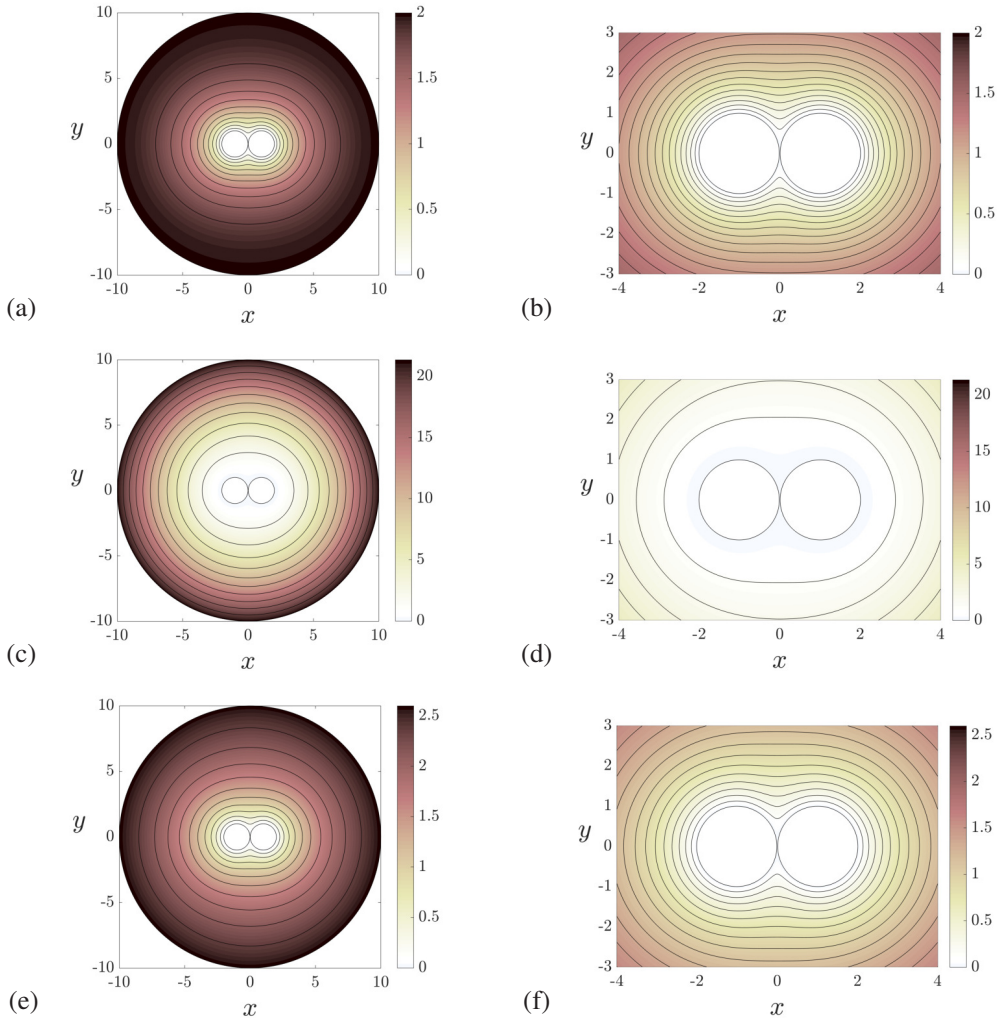


FIGURE 22. Streamlines $\psi = \text{const.}$ from the numerical solution of the Stokes problem for co-rotating cylinders with $\varepsilon = 0.01$; the outer boundary condition on $r = R_0$ is either no slip (a,b); stress-free (c,d); or (e,f) with $u_\theta = k(0.01)/R_0$, from Watson (1995) and figure 21(c).

(cf. $\mathcal{T}_s/4\pi = 1$ for a single rotating cylinder). The dashed line in figure 21(c) shows that $\mathcal{T}(0)/4\pi = 1.3734$ exactly as given by (4.11), and the agreement is evidently excellent. Just as for a single cylinder, this torque arises from the stress distribution around the entire boundary of the two cylinders, and the result cannot therefore be obtained from the lubrication theory of §4.1.

In the finite-domain numerical solution, the torque exerted on the fluid jointly by the two inner cylinders must equal the torque absorbed by the outer cylinder \mathcal{C}_0 . Figure 24 shows the dependence of this torque on R_0 (with the no-slip boundary condition) in the range $8 \leq R_0 \leq 20$, for $\varepsilon = 0.04, 0.02$ and 0.01 ; here, it is the double limiting process $R_0 \rightarrow \infty, \varepsilon \downarrow 0$ that shows convergence towards the limit 17.2587, again marked by the dashed line.

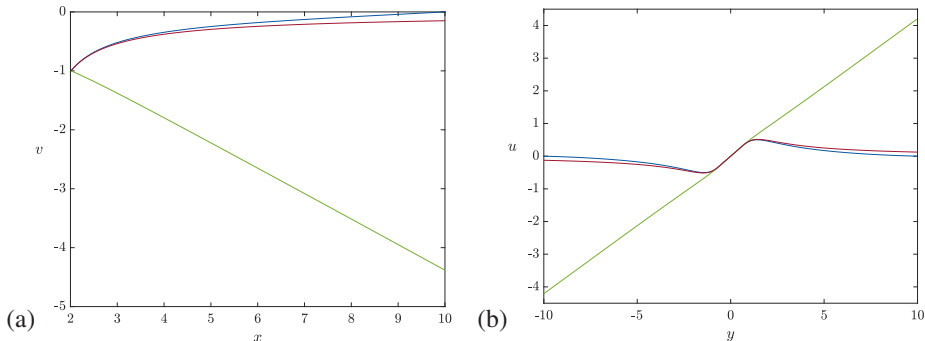


FIGURE 23. Axial velocity distributions corresponding to the streamline plots of figure 22; $\varepsilon = 0.01$: (a) $v(x, 0)$ ($2 + \varepsilon < x < 10$); (b) $u(0, y)$ ($-10 < y < 10$). The outer boundary condition on $r = R_0$ is either no slip in blue; stress-free in green; or with $u_\theta = k(0.01)/R_0$ in red. The influence of the outer boundary condition is evident: in the no-slip case, the far-field flow is that of a point vortex; in the stress-free case, it is rigid body rotation.

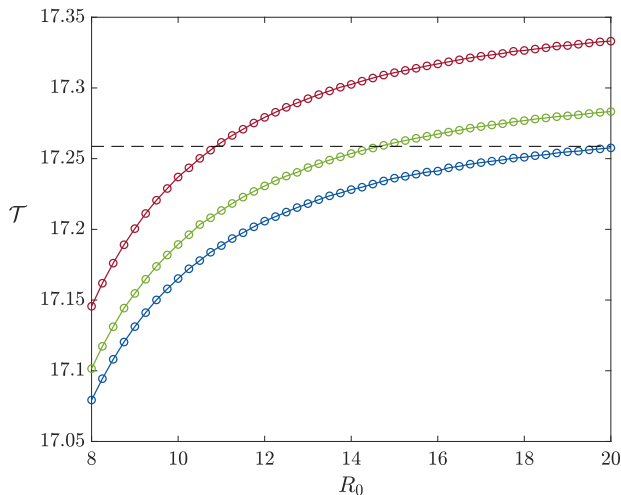


FIGURE 24. Torque on the bounding cylinder \mathcal{C}_0 (with no-slip boundary condition) as a function of R_0 for $\varepsilon = 0.04$ (red), 0.02 (green), 0.01 (blue). The double limit $R_0 \rightarrow \infty$ and $\varepsilon \downarrow 0$ is needed to approach the asymptotic value 17.2587 , marked by the dashed line, as derived in (4.11).

4.3. Analytic solution for the case of contact $\varepsilon = 0$

Just as in §2.4, we may find an analytic solution for the contact situation $\varepsilon = 0$. The function $\Psi(\xi)$ must now be even in ξ and must satisfy $\Psi = 0$, $\Psi_\xi = -1$ on $\xi = \frac{1}{2}$. The solution is $\Psi = \frac{1}{4} - \xi^2$, and the corresponding solution for $\psi(x, y)$ is

$$\psi(x, y) = (x^2 + y^2) \left(\frac{1}{4} - \frac{x^2}{(x^2 + y^2)^2} \right), \quad (4.12)$$

or, in polar coordinates

$$\psi(r, \theta) = \frac{1}{4}r^2 - \cos^2 \theta. \quad (4.13)$$

(This result may equally be found from the limit as $\varepsilon \rightarrow 0$ of the solution obtained by Jeffery's (1922) method – see Appendix A.2.) The associated cartesian velocity

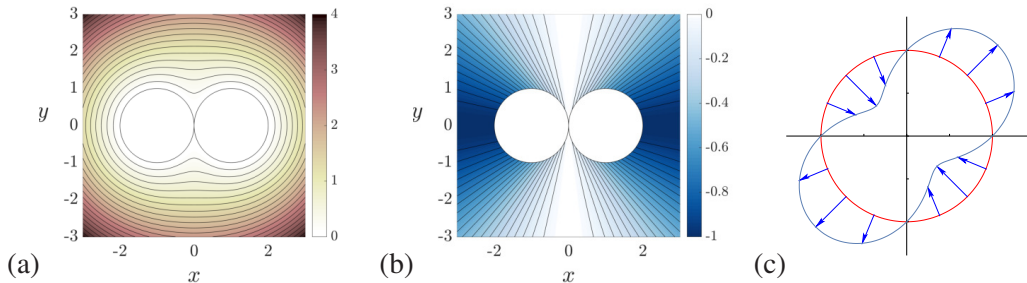


FIGURE 25. (a) Streamlines $\psi(r, \theta) = \frac{1}{4}r^2 - \cos^2 \theta = \text{const}$; (b) streamlines $\psi_Q(r, \theta) = -\cos^2 \theta = \text{const}$; (c) velocity profile for the radial quadrupole.

components are

$$u(x, y) = y \left(\frac{1}{2} + \frac{2x^2}{r^4} \right), \quad v(x, y) = -x \left(\frac{1}{2} - \frac{2y^2}{r^4} \right), \quad (4.14)$$

exhibiting the nature of the singularity as $r \rightarrow 0$. The problem here is that the first term in (4.13) corresponds to a rigid-body rotation with clockwise angular velocity $\Omega = -\frac{1}{2}$ as $r \rightarrow \infty$; this is evidently not the solution that we require, for which the velocity should tend to zero at infinity.

However, the Watson solution described in §4.2 above remains valid for arbitrarily small ε , and may be assumed to attain a limit when $\varepsilon = 0$ for which the rigid-body term is absent and the flow asymptotes to that of a virtual line vortex

$$\psi_W(x, y)|_{\varepsilon=0} \sim -1.3734 \log(1/r), \quad u_\theta(r) = -\frac{\partial \psi_W|_{\varepsilon=0}}{\partial r} \sim -\frac{1.3734}{r} \quad \text{as } r \rightarrow \infty. \quad (4.15)$$

The associated torque \mathcal{T}_0 ($= \mathcal{T}(0)$) exerted by the cylinder pair on the fluid is then given precisely by $\mathcal{T}_0 = 4\pi \times 1.3734 = 17.2587$.

4.4. Rotating frame solution; radial quadrupole

Although the solution (4.12) tends to rigid-body rotation $\Omega = -\frac{1}{2}$ at infinity, it is nevertheless not without interest. In a frame of reference rotating with this angular velocity, the cylinders ‘orbit’ with angular velocity $-\Omega = +\frac{1}{2}$. The torque \mathcal{T}_0 resisting this orbiting is just equal and opposite to the torque $-\mathcal{T}_0$ on the pair that is generated by their co-rotation. The net torque experienced by the cylinder pair (and equally the torque imparted to the fluid) is therefore zero in this situation. Figure 25(a) shows the streamlines $\psi = \text{const}$. for the flow (4.12) in the frame of the two cylinders, and figure 25(b) shows the streamlines in the frame rotating with the angular velocity $-\frac{1}{2}$; these streamlines are purely radial, the normal velocity being non-zero on the cylinders because in this rotating frame the cylinders are orbiting about the origin (as well as still rotating about their respective axes). Ciliary action of a microscopic organism could in principle generate such orbiting motion.

The streamline pattern of figure 25(b) corresponds to the streamfunction

$$\psi_Q(r, \theta) = -\cos^2 \theta = -\frac{1}{2}(1 + \cos 2\theta), \quad (4.16)$$

a very particular solution of the biharmonic equation. In the quadrant $x > 0, y > 0$, it may be recognised as the low-Reynolds-number limit of the Jeffery-Hamel flow due to a line source of strength $Q = 1$ at the intersection of the plane boundaries $x = 0, y = 0$, with no slip on both boundaries (Jeffery 1915, §4; or see, for example, Batchelor 1967,

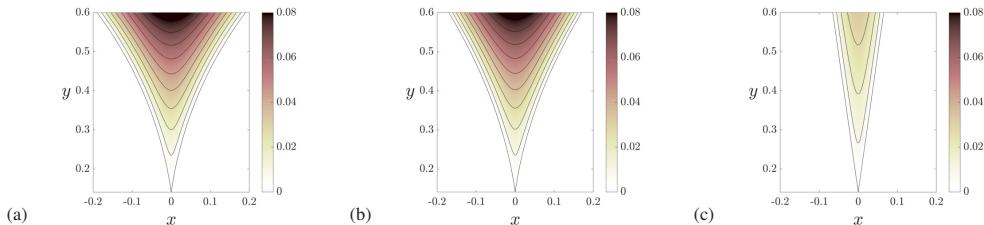


FIGURE 26. As for figure 17, but now for the co-rotating situation for $\varepsilon_1 (= -\varepsilon) = 0.01$: (a) the full numerics with no-slip boundary conditions; (b) the lubrication flow streamlines $\psi_L(x, y) = \text{const.}$ with $\psi_L(x, y)$ given by (4.2); (c) the corner flow streamlines $\psi_C(r, \theta) = \text{const.}$ with $\psi_C(r, \theta)$ given by (5.1) and with the same angle 2α at the tip, where $\alpha = 0.1413 \approx 8^\circ$.

§5.6). In the second quadrant, it represents the same flow but with a line sink $Q = -1$; and in the third and fourth quadrants, it represents again the same flows, source and sink respectively. The total velocity profile going round the circle $r = 1$ is as indicated in figure 25(c), outwards in the first and third quadrants, inwards in the second and fourth. It may be appropriate to describe this flow as a ‘radial quadrupole’.

5. The co-rotating ‘conveyor-belt’ situation when $\varepsilon < 0$

As in §3, we may consider the case $\varepsilon < 0$, which, for co-rotating cylinders, may in principle be generated by a single conveyor belt, as illustrated in figure 14(b). Setting $\varepsilon_1 = -\varepsilon > 0$, the lubrication solution of §4.1 is applicable when $0 < \varepsilon_1 \ll 1$ in the fluid region $(2\varepsilon_1)^{1/2} < |y| \ll 1$. The streamlines are shown in figure 26(a) for $\varepsilon_1 = 0.01$. For this value of ε_1 , the boundaries intersect at the point $(0, y_0)$ at angle 2α , where $y_0 = \alpha = \cosh^{-1}[1.01] \approx 0.1413 (\approx 8^\circ)$.

The corner flow analogous to (3.14) is now given by the streamfunction

$$\psi_C(r, \theta) = \frac{r(\alpha \cos \theta \sin \alpha - \theta \sin \theta \cos \alpha)}{\alpha + \cos \alpha \sin \alpha}, \quad (5.1)$$

with associated velocity components

$$u_r(\theta) = -\frac{\sin \theta(\alpha \sin \alpha + \cos \alpha) + \theta \cos \theta \cos \alpha}{\alpha + \sin \alpha \cos \alpha}, \quad u_\theta(\theta) = \frac{\theta \cos \alpha \sin \theta - \alpha \cos \theta \sin \alpha}{\alpha + \sin \alpha \cos \alpha}, \quad (5.2)$$

satisfying $u_\theta(\theta) = 0, u_r(\theta) = \pm 1$ on $\theta = \mp \alpha$ respectively. The streamlines $\psi_C(r, \theta) = \text{const.}$ are shown in figure 26(b), for angle $\alpha = 0.1413$. The pressure field for this flow satisfying the equations (3.19) is given by

$$p(r, \theta) = -\frac{2 \sin \theta \cos \alpha}{r(\alpha + \sin \alpha \cos \alpha)}. \quad (5.3)$$

The total vertical force acting on the boundary planes is zero by symmetry.

6. Conclusions

We have reinvestigated the classical problem of the Stokes flow generated by two parallel circular cylinders of unit radius, which are either (i) counter-rotating, or (ii) co-rotating. We have assumed that the fluid domain \mathfrak{D} is bounded by a cylinder $r = R_0 \gg 1$ on which the tangential velocity or tangential stress (possibly zero in either case) can be prescribed, and have provided an accurate finite-element numerical treatment of these problems.

In case (i), when the gap 2ε between the inner cylinders is small, lubrication theory provides a description of the flow in the gap region that agrees well with the numerical solution. When $\varepsilon \downarrow 0$, two saddle points at $(0, \pm(6\varepsilon)^{1/2})$ move towards the origin. When the cylinders make contact (i.e. when $\varepsilon = 0$), the domain topology changes from triply- to doubly-connected, and the two saddle points convert to two boundary-saddle points, which persist as ε is further reduced to negative values. When the outer boundary condition is either no-slip or zero-tangential-stress, the numerical evidence indicates that when $\varepsilon > 0$ the force exerted on the cylinders tends to zero as $R_0 \rightarrow \infty$; this conclusion is consistent with the lubrication analysis of §2.2.1, with the analytic solution obtained in §2.4, and with the model calculation presented in Appendix B. We have therefore been led to question Watson’s (1995) treatment of this counter-rotating problem. When $\varepsilon = 0$, there is a ‘contact force’ due to the discontinuity of pressure across the point of contact, and we have shown that the total force is continuous down to $\varepsilon = 0$ if and only if this contact force is taken into account. For $\varepsilon < 0$ (realisable as depicted in figure 14), the contact force becomes a ‘distributed contact force’ which must again be taken into account. A local corner flow similarity solution is obtained in this case, supplementing the lubrication solution that is still applicable when $|\varepsilon| \ll 1$.

In case (ii), the situation is quite different: here, the co-rotation generates a localised torque on the fluid and so a vortex-like flow $u_\theta \sim k(\varepsilon)r^{-1}$ in the far field. There is also an internally driven rigid-body rotation, but this is expunged by suitable choice of the strength of the virtual vortex (thus in effect determining the function $k(\varepsilon)$), so that the resulting velocity does as required tend to zero for large r . We have extended and refined Watson’s (1995) analysis to reveal the behaviour as $\varepsilon \downarrow 0$; in this limit, lubrication theory again describes well the highly sheared flow in the narrow gap, and good agreement is again achieved with the full numerical solution. An analytic solution has again been obtained when $\varepsilon = 0$, involving rigid-body rotation at infinity. In a frame of reference fixed in the fluid at infinity, the two cylinders orbit about each other while rotating about their respective axes. The flow in this frame is identified as a ‘radial quadrupole’, as shown in figure 25.

Acknowledgements

This research began during the Cambridge Lent Term, 2020, when ED was a Visiting Fellow at Trinity College, Cambridge; he wishes to express his gratitude to the College for the invitation that led to this visit and to the work recorded in this paper.

Appendix A. Jeffery’s (1922) solution

A.1. Counter-rotating cylinders

Defining $\xi(x, y)$, $\eta(x, y)$ and $h(\xi, \eta)$ via the conformal mapping (4.5)-(4.7), Jeffery (1922, p.173) found the streamfunction for the counter-rotating situation in the form

$$\psi_{J1}(x, y) = [h(\xi, \eta)]^{-1} [b_0 \xi (\cosh \xi - \cos \eta) + c_0 \sinh \xi + c_1 \sinh 2\xi \cos \eta], \quad (\text{A } 1)$$

where the constants b_0, c_0 and c_1 take values determined by the boundary conditions

$$b_0 = -\frac{\cosh 2\alpha}{2 \cosh \alpha \sinh^2 \alpha}, \quad c_0 = \frac{\cosh \alpha}{2 \sinh^2 \alpha}, \quad c_1 = -\frac{1}{4 \cosh \alpha \sinh^2 \alpha}. \quad (\text{A } 2)$$

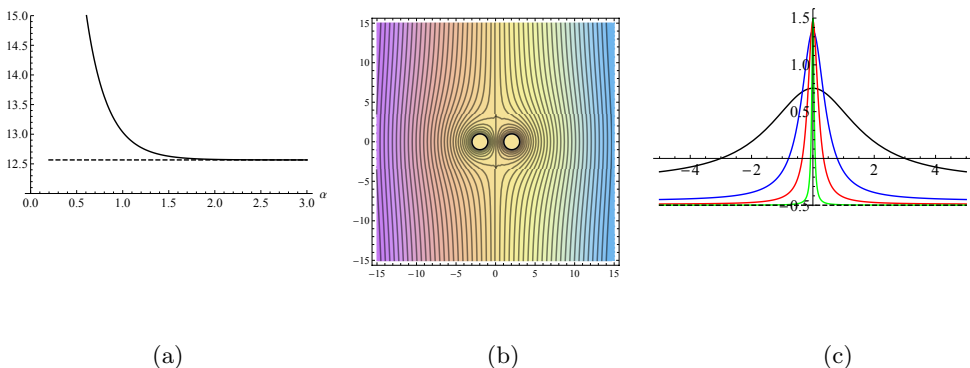


FIGURE 27. (a) The function $\mathcal{T}_2(\alpha)$ (cf. figure13(a)) showing the large- α asymptote (dashed) at the level $4\pi \approx 12.566$; (b) streamlines $\psi_{J1}(x, y, \alpha) = \text{const.}$ as given by (A 1), for the choice $\varepsilon = 1$ ($\alpha = 1.317$); for this choice, the saddle points are at $y = \pm 3$ and the flow asymptotes to the uniform stream $(-\frac{1}{4}, 0)$ as $r \rightarrow \infty$; (c) the velocity $v_{J1}(0, y, \alpha)$ for $\varepsilon = 1$ (black), 0.1 (blue), 0.2 (red) and 0.001 (green); in the limit $\varepsilon = 0$, the asymptotic uniform stream is $(-\frac{1}{2}, 0)$, as shown by the dashed line.

In polar coordinates $\{r, \theta\}$, the asymptotic form of the streamfunction ψ_{J1} for $r \gg 1$ can be expressed in the form

$$\psi_{J1}(r, \theta) \sim \frac{r \cos \theta}{2 \cosh \alpha} - \frac{(4 \cosh^2 \alpha - 1) \cos \theta + \cos 3\theta}{2r \cosh \alpha} + \text{O}(r^{-3}), \quad (\text{A } 3)$$

giving (2.25) in the limit $\alpha = 0$. The leading term in (A 3) represents a uniform stream $(0, -\frac{1}{2} \text{sech } \alpha)$ as found by Jeffery, and the term proportional to $r^{-1} \cos \theta$, which has not been previously identified, represents a torquelet of strength

$$\mu = \pi(4 \cosh^2 \alpha - 1) \text{sech } \alpha = d(\alpha) \mathcal{T}_2(\alpha)/2 \quad \text{say}, \quad (\text{A } 4)$$

where $d(\alpha)$ is the separation of virtual point torques of magnitude $\pm \mathcal{T}_2(\alpha)$ that is needed to give precisely this torquelet strength. Figure 27(a) again shows the function $\mathcal{T}_2(\alpha)$ computed from Jeffery's solution (A 1), but here in the range $\alpha \gtrsim 0.5$; this shows rapid approach to the asymptotic level 4π , this limit being quite accurately reached for $\alpha \gtrsim 2$, i.e. for $\varepsilon = \cosh \alpha - 1 \gtrsim 2.75$. The separation $d(\alpha)$ then asymptotes to $2 \cosh \alpha = 2(1 + \varepsilon)$, the distance between the centres of \mathcal{C}_1 and \mathcal{C}_2 , as might be expected.

At the other extreme $\alpha \rightarrow 0$, as we have seen from figure 13(a), $\mathcal{T}_2(\alpha) \sim 2\pi/\alpha$, so that in this limit the separation $d(\alpha)$ is given by

$$d(\alpha) \sim 6\pi/\mathcal{T}_2(\alpha) \sim 3\alpha \sim 3(2\varepsilon)^{1/2}, \quad (\text{A } 5)$$

as stated in §2.6.1.

At the intermediate value (by way of example) $\alpha = 1.317$, for which $\varepsilon \equiv \cosh \alpha - 1 = 1$, the streamlines $\psi_{J1} = \text{const.}$ are as shown in figure 27(b). For this choice of a α and ε , the saddle points are at $y = \pm 3$ and the flow settles to the uniform stream $(0, -\frac{1}{4})$ as $r \rightarrow \infty$. Moreover, $\mathcal{T}_2(1.317) = 12.70$ and d evaluates to 3.71, somewhat less than $4 (= 2(1 + \varepsilon))$, the distance between the centres of \mathcal{C}_1 and \mathcal{C}_2 . This is to be expected, because the tangential stress $\tau(\phi)$ on \mathcal{C}_2 becomes more pronounced near the gap location $\phi = \pm\pi$ as ε decreases (and similarly of course for \mathcal{C}_1).

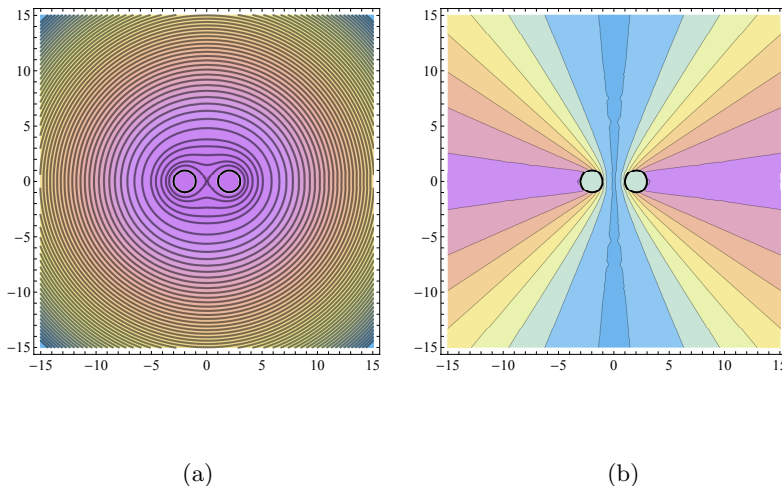


FIGURE 28. (a) Streamlines $\psi_{J2}(x, y, \alpha) = \text{const.}$ as given by (A 8), for the choice $\epsilon = 1$ ($\alpha = 1.31696$); the flow asymptotes rapidly to rigid body rotation $\Omega(\alpha) = -0.275$; (b) streamlines in rotating frame, exhibiting the radial quadrupole $\Lambda(\alpha) = -1.449$ in the far field.

Figure 27(c) shows the velocity $v_{J1}(0, y)$ on the y -axis for four choices of ϵ : 1, 0.2, 0.1, and 0.001. For large $|y|$,

$$v_{J1}(0, y) \sim -\frac{1}{2 \cosh \alpha} + \frac{2 \sinh^2 \alpha}{\cosh \alpha} y^{-2} + \text{O}(y^{-4}) = -\frac{1}{2(1+\epsilon)} + \frac{2\epsilon(2+\epsilon)}{(1+\epsilon)} y^{-2} + \text{O}(y^{-4}), \quad (\text{A } 6)$$

the leading term giving the streaming velocity $(0, -\frac{1}{2}(1+\epsilon)^{-1})$ as $|y| \rightarrow \infty$.

For $\alpha \sim (2\epsilon)^{1/2} \ll 1$ (and $r \gg \epsilon^{1/2}$, i.e. outside the lubrication zone), the solution (A 1) may be expanded in powers of ϵ ; in polar coordinates, at leading order this gives

$$\psi_{J1}(r, \theta) = \frac{1}{2} r \cos \theta - \frac{3}{2} r^{-1} \cos \theta - \frac{1}{2} r^{-1} \cos 3\theta + \text{O}(\epsilon), \quad (\text{A } 7)$$

again recovering the result (2.25) when $\epsilon = 0$.

A.2. Co-rotating cylinders

The corresponding solution for co-rotating cylinders (which we believe to be new) may be easily obtained: following Jeffery's approach the required streamfunction in this case, even in ξ , is found to be

$$\psi_{J2}(x, y) = [h(\xi, \eta)]^{-1} \left[\frac{\alpha \sinh \alpha \cosh \xi - \xi \sinh \xi \cosh \alpha}{\alpha + \cosh \alpha \sinh \alpha} \right]. \quad (\text{A } 8)$$

The streamlines for the choice $\epsilon = 1$ are shown in figure 28(a). For $r \gg 1 + \epsilon$, dropping an irrelevant constant, ψ_{J2} has the asymptotic form (in polar coordinates)

$$\psi_{J2}(r, \theta) \sim -\frac{1}{2} \Omega(\alpha) r^2 - \Lambda(\alpha) \cos^2 \theta + \text{O}(r^{-2}), \quad (\text{A } 9)$$

where

$$\Omega(\alpha) = -\frac{\alpha}{\alpha + \cosh \alpha \sinh \alpha}, \quad \Lambda(\alpha) = \frac{2 \sinh \alpha \cosh \alpha}{\alpha + \sinh \alpha \cosh \alpha}. \quad (\text{A } 10)$$

The first term represents rigid-body rotation with angular velocity $\Omega(\alpha)$, and, in the frame rotating with this angular velocity, the second term represents the instantaneous far-field radial quadrupole of strength $\Lambda(\alpha)$ apparent in figure 28(b); ‘instantaneous’ because, in this rotating frame, this field rotates in tandem with the two cylinders with angular velocity $-\Omega(\alpha)$.

Again for $\alpha \sim (2\varepsilon)^{1/2} \ll 1$ and $r \gg (2\varepsilon)^{1/2}$, ψ_{J2} has the asymptotic behaviour

$$\psi_{J2}(r, \theta) \sim \left[\frac{1}{4}r^2 - \cos^2 \theta \right] + \left[(r^2 - r^4 - 2(1 + r^2) \cos 2\theta - 2 \cos 4\theta) / 6r^2 \right] \varepsilon + O(\varepsilon^2), \quad (\text{A } 11)$$

the leading term here being exactly as found in §4.3 (equation (4.13)).

Appendix B. R_0 -dependence of force on cylinders: a simplified model

As described in §2.2.1, the computed force in the counter-rotating situation is a slowly decreasing function of the radius R_0 of the outer containing cylinder; this function depends also on the condition (no-slip or free-surface) applied on this boundary. We here seek to explain this through consideration of a simpler idealised problem that may be solved analytically, and for which the force tends to zero extremely slowly, as given by (B 9) and (B 11) below.

Suppose that the fluid is contained in the annulus between two cylinders $r = 1$ and $r = R_0$, and that the boundary conditions on the inner cylinder are

$$u_r(r, \theta) \equiv r^{-1} \partial \psi / \partial \theta = 0, \quad u_\theta(r, \theta) \equiv -\partial \psi / \partial r = -\cos \theta \quad \text{on } r = 1. \quad (\text{B } 1)$$

Thus we replace the two counter-rotating cylinders of §2 by a single cylinder with prescribed tangential velocity on its surface — a ‘squirming cylinder’ in the language of bio-fluid mechanics (Lighthill 1952, Lauga & Powers 2009); this problem has the same symmetries as the two-cylinder situation, and may be expected to give similar qualitative behaviour for large R_0 .

The general solution of $\nabla^4 \psi = 0$ proportional to $\cos \theta$ is

$$\psi(r, \theta) = (Ar + Br^{-1} + Cr \log r + Dr^3) \cos \theta, \quad (\text{B } 2)$$

giving

$$\begin{aligned} u_r(r, \theta) &= -(A + Br^{-2} + C \log r + Dr^2) \sin \theta, \\ u_\theta(r, \theta) &= -(A - Br^{-2} + C(1 + \log r) + 3Dr^2) \cos \theta. \end{aligned} \quad (\text{B } 3)$$

The boundary conditions (B 1) then give

$$A + B + D = 0, \quad A - B + C + 3D = 1. \quad (\text{B } 4)$$

The pressure $p(\theta)$ on $r = 1$ is obtained via (1.2), and the normal stress $\sigma(\theta)$ on $r = 1$ is then derived as

$$\sigma(\theta) \equiv -p(\theta) + 2d(u_r)/dr|_{r=1} = 4(B - C + D) \sin \theta. \quad (\text{B } 5)$$

Similarly, the tangential stress on $r = 1$ is

$$\tau(\theta) = r d(u_\theta/r)/dr|_{r=1} = (A - 3B - 3D) \cos \theta. \quad (\text{B } 6)$$

The vertical force on the cylinder $r = 1$ is therefore

$$F = \int_0^{2\pi} [\sigma(\theta) \sin \theta + \tau(\theta) \cos \theta] d\theta = \pi(A + B - 4C + D) = -4\pi C; \quad (\text{B } 7)$$

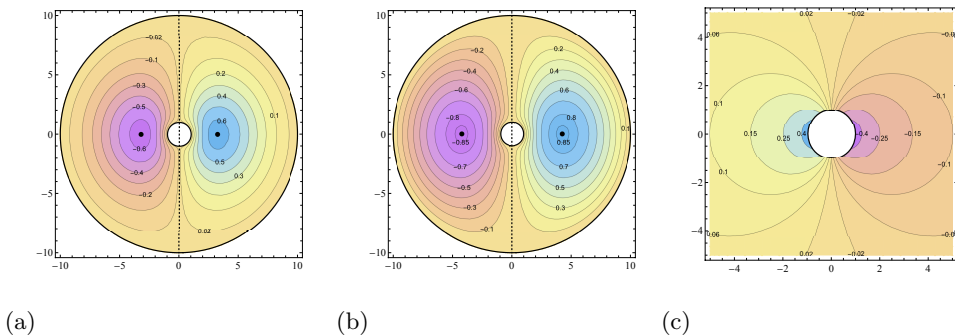


FIGURE 29. Streamlines $\psi(r, \theta) = \text{const.}$ for the flow (B 2); (a) with no slip on $r = R_0$ (here = 10); (b) with zero tangential stress on $r = R_0$; in both cases, there are two elliptic points marked by the bullets, and four half-saddles, so $n_e = 2, n_s = 2$ and $n_e - n_s = N_E(\Omega) = 0$, the domain Ω being doubly-connected; (c) with no outer boundary condition ($C = D = 0$), and with $A = 0$ thus showing the instantaneous (dipole) flow in a frame fixed to the fluid at infinity.

the cylinder therefore exerts a force $-F = 4\pi C$ on the fluid, and it is this force that provides the stokeslet ingredient $C r \log r \cos \theta$ in (B 2).

No-slip on $r = R_0$

In this case we have the additional boundary conditions $u_r = u_\theta = 0$ on $r = R_0$, giving

$$A + B R_0^{-2} + C \log R_0 + D R_0^2 = 0, \quad A - B R_0^{-2} + C(1 + \log R_0) + 3D R_0^2 = 0. \quad (\text{B } 8)$$

We solve (B 4) and (B 8) for the constants A, B, C, D and then from (B 7) we have the force F as a function of R_0 in the form

$$F_{\text{noslip}}(R_0) = \frac{2\pi(R_0^2 - 1)}{1 - R_0^2 + (1 + R_0^2) \log R_0} \sim \frac{2\pi}{\log R_0 - 1} \quad \text{as } R_0 \rightarrow \infty, \quad (\text{B } 9)$$

with very slow logarithmic convergence to zero as $R_0 \rightarrow \infty$. The streamlines for this flow are shown in figure 29(a) for the choice $R_0 = 10$.

Zero tangential stress on $r = R_0$

In this case, the boundary conditions on $r = R_0$ are $u_r = 0$ and $d(u_\theta/r)/dr = 0$, giving

$$A + B R_0^{-2} + C \log R_0 + D R_0^2 = 0, \quad -A + 3B R_0^{-2} - C \log R_0 + 3D R_0^2 = 0, \quad (\text{B } 10)$$

which again may be solved together with (B 4) for A, B, C, D . The expression for the force in this case is

$$F_{\text{zerostress}}(R_0) = \frac{4\pi(R_0^4 - 1)}{1 - R_0^4 + 2(1 + R_0^4) \log R_0} \sim \frac{4\pi}{2 \log R_0 - 1} \quad \text{as } R_0 \rightarrow \infty, \quad (\text{B } 11)$$

with again very slow convergence to zero as $R_0 \rightarrow \infty$. The streamlines for this case are shown in figure 29(b), in which the more rapid flow near the boundary $r = R_0$, indicated by the closeness of the streamlines, is evident.

We may note further that

$$F_{\text{noslip}}(R_0) - F_{\text{zerostress}}(R_0) \sim \pi(\log R_0)^{-2} \quad \text{as } R_0 \rightarrow \infty. \quad (\text{B } 12)$$

No outer boundary

If we take $C = D = 0$ in (B 2), thus eliminating the terms that are most divergent

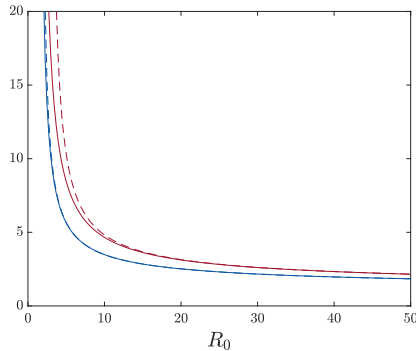


FIGURE 30. Curves of $F_{\text{noslip}}(R_0)$ (red, B 9) and $F_{\text{zerostress}}(R_0)$ (blue, B 11), with the corresponding asymptotic curves shown dashed; both curves tend very slowly to zero (like $1/\log R_0$) with increasing R_0 .

for large r , then we have simply $A = -B = \frac{1}{2}$, and the flow is a simple potential flow; figure 29(c) shows the instantaneous streamlines in a frame of reference fixed to the fluid at infinity; this is a dipole field. It is interesting that this ‘swimming flow’ could be generated by ciliary action on the surface of a microscopic organism; in contrast to the conventional Stokes flow past a cylinder, the force here evaluates to zero, because the force generated by the ciliary action (B 1) is exactly balanced by the resulting drag force on the organism.

The contours $\psi(r, \theta) = \text{const.}$ for these three flows are shown in figure 29, and the curves of $F_{\text{noslip}}(R_0)$ and $F_{\text{zerostress}}(R_0)$ are shown in figure 30. The asymptotic forms, shown dashed, provide a very good approximation for $R_0 \gtrsim 10$.

Appendix C. Asymptotic analysis of Watson’s (1995) solution

Watson’s (1995) solution of the co-rotating problem involved the function

$$S(\alpha) = \frac{1}{2} + \frac{\alpha \sinh^2 \alpha \tanh \alpha}{\alpha + \sinh \alpha \cosh \alpha} - 4 \sum_{n=2}^{\infty} \frac{\sinh \alpha (\sinh \alpha + n \cosh \alpha) + n e^{-n\alpha} \sinh n\alpha}{(n^2 - 1)(n \sinh 2\alpha + \sinh 2n\alpha)}. \quad (\text{C } 1)$$

The convergence of the sum here is an issue of immediate concern. For any fixed $\alpha > 0$, the coefficient in the n th term of the sum is proportional to $n^{-1} e^{-2n\alpha}$ for large n , so that convergence is assured. However, as $\alpha \rightarrow 0$, more and more terms of the series must be retained to get any prescribed level of accuracy. Defining $S[N, \alpha]$ as the function (C 1), when the summation is truncated at $n = N$, figure 31(a) shows log-log plots of $S[N, \alpha]$, for $N = 10, 10^2, 10^3, 10^4$. The dashed line has slope 2, indicating that, as $N \rightarrow \infty$, $S[N, \alpha] \sim k \alpha^2$ for some constant k . Figure 31(b) shows the functions $S[10^3, \alpha]/\alpha^2$ and $S[10^4, \alpha]/\alpha^2$, indicating that $k = 0.7281$ to good approximation. As expected, this behaviour breaks down when α is too small ($\lesssim 0.001$ when $N = 10^4$), but it nevertheless indicates that the limiting function $S(\alpha)$ has an asymptotic behaviour that may be adopted in the form

$$S(\alpha) \sim 0.7281 \alpha^2 \quad \text{as } \alpha \rightarrow 0. \quad (\text{C } 2)$$

A second function $K(\alpha)$ is then defined by

$$K(\alpha) = \frac{\alpha}{S(\alpha)(\alpha + \sinh \alpha \cosh \alpha)}, \quad (\text{C } 3)$$

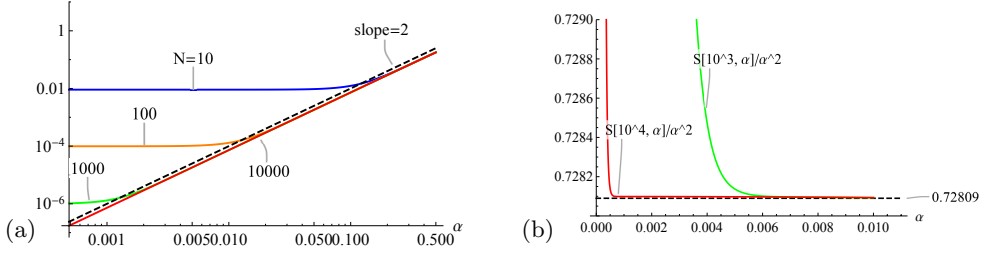


FIGURE 31. (a) Log-log plots of the functions $S[N, \alpha]$ for $N = 10, 10^2, 10^3, 10^4$, indicating that $S[N, \alpha] \sim k \alpha^2$ over a range of α that extends towards $\alpha = 0$ with increasing N ; (b) plots of $\alpha^{-2} S[N, \alpha]$ for $N = 10^3, 10^4$, indicating that $k \approx 0.7281$.

with the asymptotic behaviour that follows from (C 2),

$$K(\alpha) \sim 0.6867\alpha^{-2} \quad \text{as } \alpha \rightarrow 0; \quad (\text{C 4})$$

(and actually $\alpha^2 K(\alpha) < 0.6868$ for all $\alpha \geq 0$).

In view of the symmetry, we may restrict attention to the half-space $x \geq 0$, and to the fluid region $0 \leq \xi < \alpha$. With $\xi(x, y)$, $\eta(x, y)$ and $h(\xi, \eta)$ defined by (4.6) and (4.7), Watson's streamfunction is given by

$$\psi_W(x, y) = -c h[\xi(x, y), \eta(x, y)]^{-1} \phi[\xi(x, y), \eta(x, y)], \quad (\text{C 5})$$

where $\phi(\xi, \eta)$ has the Fourier series representation

$$\begin{aligned} \phi(\xi, \eta) = & K(\alpha)(\cosh \xi - \cos \eta) \log(2 \cosh \xi - 2 \cos \eta) + a_0(\alpha) \cosh \xi + b_0(\alpha) \xi \sinh \xi \\ & + \sum_{n=1}^{\infty} [a_n(\alpha) \cosh(n+1)\xi + b_n(\alpha) \cosh(n-1)\xi] \cos n\eta. \end{aligned} \quad (\text{C 6})$$

Here the coefficients are given by

$$a_0(\alpha) = -\frac{\alpha + K(\alpha)(\alpha + \alpha^2 + e^{-\alpha} \sinh \alpha)}{\alpha + \sinh \alpha \cosh \alpha}, \quad b_0(\alpha) = \frac{\coth \alpha - K(\alpha) \sinh^2 \alpha}{\alpha + \sinh \alpha \cosh \alpha}, \quad (\text{C 7})$$

$$a_1(\alpha) = \frac{1}{2} K(\alpha) e^{-\alpha} \operatorname{sech} \alpha, \quad b_1(\alpha) = K(\alpha) \left(1 + \alpha - \frac{1}{2} \tanh \alpha\right), \quad (\text{C 8})$$

and, for $n \geq 2$,

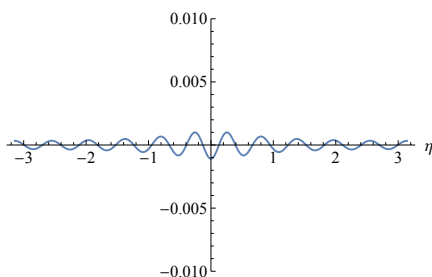
$$a_n(\alpha) = \frac{2K(\alpha)(ne^{-\alpha} \sinh \alpha + e^{-n\alpha} \sinh n\alpha)}{n(n+1)(\sinh 2n\alpha + n \sinh 2\alpha)}, \quad b_n(\alpha) = -\frac{2K(\alpha)(ne^{\alpha} \sinh \alpha + e^{-n\alpha} \sinh n\alpha)}{n(n-1)(\sinh 2n\alpha + n \sinh 2\alpha)}. \quad (\text{C 9})$$

Again, for any fixed $\alpha > 0$, these coefficients have the asymptotic behaviour

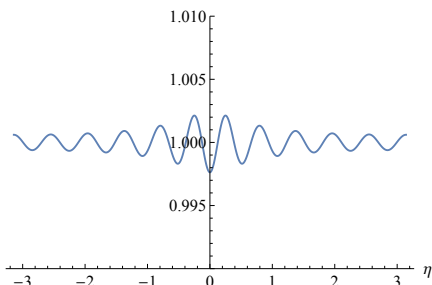
$$a_n(\alpha) \sim \frac{4K(\alpha)e^{-\alpha} \sinh \alpha}{n e^{2n\alpha}}, \quad b_n(\alpha) \sim -\frac{4K(\alpha)e^{\alpha} \sinh \alpha}{n e^{2n\alpha}} \quad \text{as } n \rightarrow \infty, \quad (\text{C 10})$$

so that the coefficient of $\cos n\eta$ in (C 6) has the behaviour

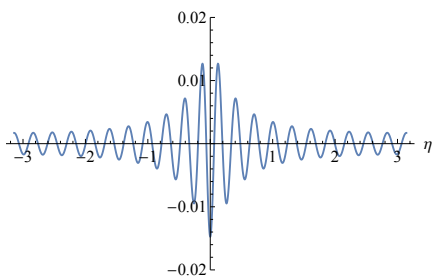
$$[a_n(\alpha) \cosh(n+1)\xi + b_n(\alpha) \cosh(n-1)\xi] \sim \frac{4K(\alpha)}{n e^{(n-1)(\alpha-\xi)} e^{n\alpha}} \quad \text{as } n \rightarrow \infty. \quad (\text{C 11})$$



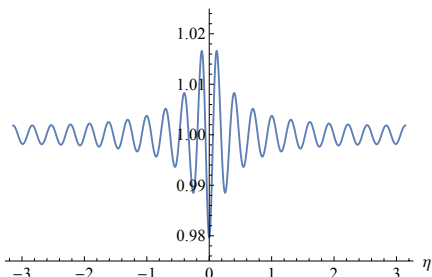
(a)



(b)



(c)



(d)

FIGURE 32. Verification of the impermeability and no-slip conditions (C 12) on $\xi = \alpha$; (a) and (b): $\phi(\alpha, \eta)/\phi(0, \pi)$ and $\sinh \alpha \partial \phi / \partial \xi|_{\xi=\alpha}$; $\alpha = 0.4583, N = 10, \phi(0, \pi) = -0.4681$; (c) and (d): the same for $\alpha = 0.1413, N = 20, \phi(0, \pi) = -0.4972$.

The series in (C 6) therefore converges exponentially rapidly for $0 \leq \xi \leq \alpha$, and may again be evaluated to good approximation if terminated at $n = N$ provided N is appropriately chosen in relation to α . Recalling that $\alpha = (2\varepsilon)^{1/2}$, we therefore need $N \gg (2\varepsilon)^{-1/2}$. When $\varepsilon = 0.1$, this requirement is simply $N \gg 1$; we actually ran to $N = 1000$ in constructing figures 20 and 21, thus providing extreme accuracy. If $N = 10$ is used instead, the resulting figures are just as good at this value of ε , but if ε is reduced, N must be correspondingly increased to maintain accuracy.

The definitions (C7) – (C9) ensure that the impermeability and no-slip conditions are satisfied on the co-rotating cylinders $\xi = \pm\alpha$. These conditions are

$$\phi(\alpha, \eta) = 0 \quad \text{and} \quad \sinh \alpha \left. \frac{\partial \phi}{\partial \xi} \right|_{\xi=\alpha} = 1 \quad \text{for} \quad -\pi < \eta \leq \pi. \quad (\text{C } 12)$$

Normalising $\phi(\alpha, \eta)$ by its value at $\xi = 0, \eta = \pi$ (corresponding to the point $x = 0, y = 0$), figure (32) shows $\phi(\alpha, \eta)/\phi(0, \pi)$ and $\sinh \alpha \partial\phi/\partial\xi|_{\xi=\alpha}$, evaluated for two cases: $\varepsilon = 0.1$ ($\alpha = 0.4583$) truncating the series at $N = 10$; and $\varepsilon = 0.01$ ($\alpha = 0.1413$) truncating the series at $N = 20$. The conditions are satisfied to well within 0.2% and 2% accuracy respectively at these levels of truncation. As ε is further decreased, N must be correspondingly increased to retain accuracy.

The coefficient of the ‘rigid-body’ term in the solution as $r \rightarrow \infty$ (i.e. as $\xi^2 + \eta^2 \rightarrow 0$) is proportional to

$$R(\alpha) \equiv a_0(\alpha) + \sum_{n=1}^{\infty} [a_n(\alpha) + b_n(\alpha)], \quad (\text{C } 13)$$

and it is the condition $R(\alpha) \equiv 0$ that actually determines the function $K(\alpha)$ (through equations (C1), (C3) above). Provided the same N is chosen in (C1) and (C6), this condition is actually identically satisfied for any N , as may be verified with some effort.

Appendix D. Numerical modelling

Finite elements were used to determine the Stokes flow in the triply-connected domain \mathfrak{D} between the outer boundary circular cylinder \mathcal{C}_0 and the inner cylinders $\mathcal{C}_{1,2}$. On \mathcal{C}_0 the no-slip condition

$$\mathbf{u}|_0 = 0 \quad (\text{D } 1)$$

was adopted for most simulations. On $\mathcal{C}_{1,2}$, the boundary conditions correspond to rotation with no slip, i.e.

$$\mathbf{u}|_{\{1,2\}} = \omega_{\{1,2\}} \mathbf{e}_z \wedge \mathbf{n}, \quad (\text{D } 2)$$

where \mathbf{n} is the unit outward normal on $\mathcal{C}_{1,2}$. These boundary conditions are called ‘essential’ in finite-element terms (i.e. they are imposed explicitly on the solution \mathbf{u}).

The finite-element formulation involves writing the equations in variational form; it is then required to find \mathbf{u} in \mathcal{W}_{bc} and p in \mathcal{Q} such that

$$2 \int_{\mathfrak{D}} \mathbf{e}(\mathbf{u}) : \mathbf{e}(\mathbf{w}) \, d\mathbf{x} - \int_{\mathfrak{D}} p \nabla \cdot \mathbf{w} \, d\mathbf{x} = 0, \quad \forall \mathbf{w} \in \mathcal{W}_0, \quad (\text{D } 3a)$$

$$\int_{\mathfrak{D}} q \nabla \cdot \mathbf{u} \, d\mathbf{x} = 0, \quad \forall q \in \mathcal{Q}, \quad (\text{D } 3b)$$

where $\mathbf{e}(\mathbf{u})$ is the rate-of-strain tensor, with cartesian components e_{ij} , and \mathcal{W}_{bc} , \mathcal{W}_0 and \mathcal{Q} are suitably defined function spaces,

$$\mathcal{W}_{bc} = \left\{ \mathbf{w} \in [H^1(\mathfrak{D})]^2 : \mathbf{w}|_{\{0,1,2\}} = \mathbf{u}|_{\{0,1,2\}} \right\}, \quad (\text{D } 4a)$$

$$\mathcal{W}_0 = \left\{ \mathbf{w} \in [H^1(\mathfrak{D})]^2 : \mathbf{w}|_{\{0,1,2\}} = 0 \right\} \quad \text{and} \quad \mathcal{Q} = \left\{ q \in L^2(\mathfrak{D}) : \langle q \rangle_{\mathfrak{D}} = 0 \right\}. \quad (\text{D } 4b)$$

\mathcal{Q} consists of functions with zero mean on \mathfrak{D} ; this allows for the fact that the pressure is determined only up to an arbitrary constant. These function spaces are then approximated with discrete spaces, here by a triangular mesh, and with quadratic elements

for the velocity and affine elements for pressure. The resulting system was solved using *FreeFem++* (Hecht 2012).

In the streamfunction formulation, since the domain is not simply connected, ψ can be set to zero on only one boundary.

In the case of counter-rotating cylinders, we set $\psi|_0 = 0$ on \mathcal{C}_0 . The value of ψ on \mathcal{C}_1 and \mathcal{C}_2 is not known *a priori*. These missing boundary conditions can however be recovered from the solution of (D3) as

$$\psi_{\{1,2\}} = \pm \frac{1}{2}Q \quad \text{with} \quad Q = \int_{-\varepsilon}^{\varepsilon} v(x, 0) dx, \quad (\text{D5})$$

and by solving

$$\nabla^2 \psi = (\nabla \wedge \mathbf{u}) \cdot \mathbf{e}_z \quad \text{with} \quad \psi|_{\{0,1,2\}} = \psi_{\{0,1,2\}}; \quad (\text{D6})$$

or equivalently (but with higher-order shape functions) by solving (1.3) with the additional boundary conditions

$$\mathbf{n} \cdot \nabla \psi|_{\{1,2\}} = \omega_{\{1,2\}}. \quad (\text{D7})$$

In the co-rotating case, the value of ψ is by symmetry the same on \mathcal{C}_1 and \mathcal{C}_2 , we chose for convenience to set $\psi|_{1,2} = 0$. The value of ψ on \mathcal{C}_0 is then determined as

$$\psi|_0 = \int_{-R_0}^{-2-\varepsilon} v(x, 0) dx = - \int_{2+\varepsilon}^{R_0} v(x, 0) dx. \quad (\text{D8})$$

Some simulations using a stress-free outer boundary were also carried out. In that case (D1) is replaced by conditions that are in general non-trivial to implement, namely

$$\mathbf{n} \cdot \mathbf{u}|_0 = 0, \quad \mathbf{n} \cdot \mathbf{e}(\mathbf{u}) \cdot \mathbf{t}|_0 = 0, \quad (\text{D9})$$

where \mathbf{n} and \mathbf{t} are unit normal and tangent vectors on \mathcal{C}_0 . In writing the variational form for this problem, the conditions on $\mathbf{w}|_{\{0\}}$ must be relaxed for both \mathcal{W}_{bc} and \mathcal{W}_0 . Since the full rate-of-strain tensor \mathbf{e} was retained in the numerical formulation, the integration by parts that yields (D3a) remains valid as stated with the boundary conditions (D9). The impenetrability condition is ‘essential’, and needs to be imposed strongly by a penalisation of the minimisation problem (D3) with

$$\oint_{\mathcal{C}_0} (\mathbf{n} \cdot \mathbf{u})(\mathbf{n} \cdot \mathbf{w}) ds, \quad (\text{D10})$$

where s is arclength on \mathcal{C}_0 , whereas the condition that $\mathbf{n} \cdot \mathbf{e}(\mathbf{u}) \cdot \mathbf{t}|_0 = 0$ is ‘natural’ and follows from the weak form (D3).

Finally, in order to resolve variables with sufficient accuracy over the full range of scales $[\varepsilon, R_0]$, an Uzawa splitting was employed in our largest simulations, in order to reduce matrix sizes.

REFERENCES

- BATCHELOR, G. K. 1967 *An Introduction to Fluid Dynamics*. Camb. Univ. Press.
- BICKLEY, W.G. 1937 LXXIII. The plane jet. *Phil. Mag.* **23**:156, 727-731, doi.org/10.1080/14786443708561847
- BOYLAND, P.L., AREF, H. & STREMLER, M.A. 2000 Topological fluid mechanics of stirring. *J. Fluid Mech.* **403**, 277-304.
- DORREPAAL, J.M., O’NEILL, M.E. & RANGER, K.B. 1984 Two-dimensional Stokes flows with cylinders and line singularities. *Mathematika* **31**, 65-75.
- ELLIOTT, L., INGHAM, D.B. & EL BASHIR, T.B.A. 1995a The solution of a paradoxical slow

- flow problem using a boundary element method. *Eng. Anal. with Boundary Elements* **15**, 29–35.
- ELLIOTT, L., INGHAM, D.B. & EL BASHIR, T.B.A. 1995b Stokes flow past two circular cylinders using a boundary element method. *Computers & Fluids*. **24**, 787–798.
- HECHT, F. 2012 New development in freefem++. *J. Numer. Math.* **20**, 251–265. <https://doi.org/10.1515/jnum-2012-0013>
- HERTZ, H. 1882 Contact between solid elastic bodies. *J. für die Reine und Angew. Math.* **92**.
- HILLS, C.P. 2002 Flow patterns in a tworoll mill. *Quart. J. Mech. Appl. Math. A* **55**, 2, 273296. doi.org/10.1093/qjmam/55.2.273
- JANA, S.C., METCALFE, G. & OTTINO, J.M. 1994 Experimental and computational studies of mixing in complex Stokes flows: the vortex mixing flow and multicellular cavity flows. *J. Fluid Mech.* **269**, 199–246.
- JEFFERY, G.B. 1915 The two-dimensional steady flow of a viscous fluid. *Phil. Mag. A* **29**:172, 455–465. doi.org/10.1080/14786440408635327
- JEFFERY, G.B. 1922 The rotation of two circular cylinders in a viscous fluid. *Proc. Roy. Soc. A* **101**, 169–174.
- LAMB, H. 1932 *Hydrodynamics*. Camb. Univ. Press.
- LAUGA, E. & POWERS, T.R. 2009 The hydrodynamics of swimming microorganisms. *Rep. Prog. Phys.* **72** (9), 096601. doi = 10.1088/0034-4885/72/9/096601
- LIGHTHILL, M.J. 1952 On the squirring motion of nearly spherical deformable bodies through liquids at very small Reynolds numbers. *Commun. Pure Appl. Math.* **109**, 109–118.
- PROUDMAN, I. & PEARSON, J.R.A. 1957 Expansions at small Reynolds numbers for the flow past a sphere and a circular cylinder. *J. Fluid Mech.* **2**, 237–262.
- SCHUBERT, G. 1967 Viscous flow near a cusped corner. *J. Fluid Mech.* **27**, 647–656.
- SMITH, S.H. 1991 The rotation of two circular cylinders in a viscous fluid. *Mathematika* **38**, 63–66.
- TAYLOR, G.I. 1962 On scraping viscous fluid from a plane surface. *The Scientific Papers of Sir Geoffrey Ingram Taylor, vol. IV* (ed. G. K. Batchelor), 410413. Camb. Univ. Press.
- UEDA, Y., SELIER, A., KIDA, T. & NAKANISHI, M. 2003 On the low-Reynolds-number flow about two rotating circular cylinders. *J. Fluid Mech.* **495**, 255–281. doi: 10.1017/S002211200300627X
- WATSON, E.J. 1995 The rotation of two circular cylinders in a viscous fluid. *Mathematika* **42**, 105–126.